(2)

Contract No.: F49620-90-C-0061
SRA No.: R91-910032-F

Final Report
Period: 25 July 1990 - 24 Jan. 1991

QUANTUM DEVICES AND STRUCTURES

H. L. Grubin and T. R. Govindan

Scientific Research Associates, Inc.
P. O. Box 1058
Glastonbury, CT 06033

Prepared for

Air Force Office of Scientific Research
Bolling Air Force Base, D.C.

March 1991

Scientific Research Associates, Inc.
P. O. Box 1058
Glastonbury, CT 06033

REPORT DOCUMENTATION PAGE

Form Approved
OMB No. 0704-0188

1. AGENCY USE ONLY (Leave blank)	2. REPORT DATE	3. REPORT TYPE AND DATES COVERED
	26 March 1991	Final, 25 July 1990-24 January 1991

4. TITLE AND SUBTITLE

Quantum Devices and Structures

5. FUNDING NUMBERS

F49620-90-C-0061

6. AUTHOR(S)

H. L. Grubin and T. R. Govindan

7. PERFORMING ORGANIZATION NAME(S) AND ADDRESS(ES)

Scientific Research Associates, Inc.
50 Nye Road, P.O. Box 1058
Glastonbury, CT 06033

8. PERFORMING ORGANIZATION REPORT NUMBER

R-91-910032-F

9. SPONSORING/MONITORING AGENCY NAME(S) AND ADDRESS(ES)

Air Force Office of Scientific Research
Building 410
Bolling AFB, DC 20332-6448

G.W.H

10. SPONSORING/MONITORING AGENCY REPORT NUMBER

3005/A1

11. SUPPLEMENTARY NOTES

12a. DISTRIBUTION/AVAILABILITY STATEMENT

Approved for public release;
distribution unlimited.

12b. DISTRIBUTION CODE

13. ABSTRACT *(Maximum 200 words)*

All devices constructed from quantum mechanical resonant tunneling structures are dependant upon their ability to move charge in and out of the quantum well. The ability to effectively modulate this charge is dependent upon the device structure; which in turn depends upon an understanding of quantum device physics; which in turn depends upon device theory, simulation, and experiment. In the present study, Scientific Research Associates, Inc. implemented its time-dependent quantum Liouville equation algorithm for obtaining the density matrix in the coordinate representation. Switching times as well as response times to ac signals were determined for tunneling structures with variable charge densities. A recommended future program involves implementing the algorithm for designing three proto-typical tunneling devices, and determining the limits of operation. These devices are: (1) a resonant tunneling self-excited, high-frequency local oscillator, (2) a resonant tunneling high-speed photo-induced two-terminal electrical switching element, and (3) a "permeable base like" resonant tunneling high current-level three terminal switching transistor.

14. SUBJECT TERMS	15. NUMBER OF PAGES
Liouville equation, density matrix, resonant tunneling diodes	35
	16. PRICE CODE

17. SECURITY CLASSIFICATION OF REPORT	18. SECURITY CLASSIFICATION OF THIS PAGE	19. SECURITY CLASSIFICATION OF ABSTRACT	20. LIMITATION OF ABSTRACT
Unclassified	Unclassified	Unclassified	UL

1. Introduction

"... Resonance implies the presence inside the well of a certain amount of carriers which, at least in the most common experimental situations, are not there at the beginning. When dealing with electrons, this means that a space charge builds up. If the resonant eigenstate can accommodate enough charge this affects the potential energy making it time dependent and giving rise to a feedback mechanism linking the changes in potential energy with carrier trapping." This prescient statement by Ricco and Azbel (1984) is at the heart of the operation of all quantum device structures incorporating resonant tunneling contributions, and the means by which this feedback mechanism occurs is at the core of virtually all measurement and theory of quantum structures. It suggests that all devices constructed from resonant tunneling structures are dependent on the ability to move charge in and out of the resonant tunneling quantum well. **How is this charge distributed? Once the distribution of charge is determined how are we to manipulate the spatial positions of the charge, and within what time constraints, to advantageously design devices?** This last question was at the core of the Phase I SBIR study; the results of which are discussed in the sections below. Before this discussion, we note that at least three significant device applications have emerged from the capabilities and physics addressed during the Phase I study. These include: (1) The design of a resonant tunneling diode (RTD) self excited oscillator, (2) the design of an optically induced high speed RTD switch and (3) the design of a high current level three terminal RTD transistor. Each separate application forms part of a recommended future study.

To establish what all quantum transport RTD theory must describe we first summarize the experimental state of understanding of RTD. We turn to the results of Eaves and Co-workers (1989), and point out, as is often the case, that the interpretation rests heavily on adjunct computations performed incorporating Schrodinger's equation coupled to a assumed distribution of carriers. All results are steady state results.

The detailed experiments of Eaves and Co-workers (1989) were performed on asymmetric structures; and while we would like to see similar detailed experiments performed on symmetric structures, the essential physics is likely to be independent of this asymmetry.

The band structure, current-voltage characteristics, and areal distribution of charge within the structure are displayed in figures 1a through 1c. The salient features of these measurements and additional ones discussed in Eaves and co-workers (1989) are:

(1) The threshold voltage at which resonant tunneling and current begins to flow, V_{th}, occurs at values below the voltage at peak current, V_p.

(2) Resonant tunneling occurs when the energies in the bound state of the accumulation layer on the emitter side of the double barrier, and the quantum well essentially coincide.

(3) The screening effect of the charge buildup in the quantum well is responsible for the extended voltage range over which resonant tunneling is observed.

(4) When the applied voltage is between V_{th} and V_p, only a very small voltage change across the emitter barrier is needed to charge up the well. Due to the screening effect of the charge, almost all the extra voltage drop falls across the collector barrier and the depletion layer.

(5) The rates at which carriers enter the quantum well into the quasi bound state are different than the rates at which carriers leave the quantum well and tunnel to the emitter. Tunnelling takes place at a fixed energy. The implication is that conservation of transverse energy under bias does not occur. If the storage time in the well is very long (> 1 ps) carriers are likely to achieve thermalization. The parameters of thermalization are electron temperature and quasi-Fermi level with a Fermi level in the quantum well that is different from that of the emitter.

(6) As V increases above V_p a transition occurs in which charge is expelled from the quantum well. Further increases in bias result in increases in charge on the emitter side of the barrier.

The above discussion of Eaves and coworkers (1989) suggests two distinct contributions to the electric characteristics of resonant tunneling structures. **First,** coherent scattering of the type similar to Fabry-Perot scattering; **second,** incoherent contributions arising form carrier-carrier scattering and perhaps, e.g., phonon scattering. At any bias level contributions of each are expected, and the issues include determining the relative weights of each. Detailed analysis under the Phase I study tends to confirm these conclusions.

But the analysis of Eaves and co-workers (1989) rest on relatively straightforward applications of Schrodinger's equations and Poisson's equation with intuitive approaches to temporal constraints and does not provide a simulation tool for extracting the essential time dependence of quantum device physics. Indeed **the engineering and physics community requires** for the successful development of quantum device structures, **the quantum transport equivalent to the drift and diffusion equations!** Scientific Research Associates, Inc. (SRA) has been developing such programs and the Phase I SBIR study was involved in further development and implementation of its time dependent algorithm for determining the transient behavior of resonant tunneling structures. The unique feature of the study was the implementation of SRAs algorithm for solving the time dependent Liouville equation. The motivations for this as discussed in the Phase I proposal were as follows:

"...one of the more significant aspects of quantum device behavior is its time dependence and the mixing of quantum states. Here conventional approaches of analyzing this phenomena generally involve the evaluation of eigenstates and perturbations thereof. While these approaches are not incorrect, they are unlikely to yield useful information when the perturbations significantly depart from equilibrium. Implicit in the approach of analyzing quantum phenomena are the equations used. ... Presently, with few exceptions, see, e.g., Frensley (1987), most descriptions of quantum device behavior involving large numbers of carriers are based upon the single particle Schrodinger equation. This, is inadequate, as discussed by Frensley (1985) in that **temperature effects, time dependent phenomena and dissipative effects are not a natural part of the governing single particle equations.** Self-consistency is also an issue. Further, if all of these deficiencies could be overcome the quantum transport algorithms should be available to a broad range of scientists and engineers. To paraphrase Iafrate (1989) 'user-friendly' quantum mechanical algorithms are needed to provide a basis for much of the new quantum based devices".

The specific technical objectives of the Phase I study were represented by the tasks of the Statement of Work. These included:

(1) Applying the density matrix algorithm for solving the time dependent Liouville equation, coupled to Poisson's equation to calculate the steady state characteristics of RTDs;

(2) Calculate the time dependent behavior when a small ac signal is superimposed upon the dc result;

(3) Examine the time dependent behavior when the applied frequency correspond to the sum and difference frequencies of the quasi bound states.

Each of these tasks was completed. In addition calculations were performed to determine the time it takes to fill and empty a quantum well. Time constants associated with the transient behavior of the device were estimated. For a GaAs/AlGaAs structure the time to fill and empty the quantum well was estimated as 500fs. Thus oscillations in the terahertz range are feasible. Additionally dc calculations were performed for a structure that is generically similar to the indium based quantum well that has resulted in large peak to valley ratios.

The issues that needed to be addressed with respect to resonant tunneling structures were:

(1) the physics of charge filling and emptying of the quantum well;

(2) the time constants associated with the filling and emptying of the quantum well,

(3) the material parameters associated with the structure;

(4) and simultaneously the applications of the RTD.

Under the Phase I SBIR study issues (1) and (2) were addressed through numerical simulation. The numerical simulation program which has been under development at SRA for several years, with support from several research funding agencies, including AFOSR under which the Liouville algorithm was initially developed, represents a significant advance over simulations undertaken before. It is recommended that in a future study, issues (1) and (2) should be continued but the emphasis should be on issues (3) and (4).

2. Governing Equations

The density matrix, ρ, satisfies the Liouville equation of motion:

$$(1) \qquad i\hbar\,\partial\rho/\partial t = [H,\rho]$$

where H is the Hamiltonian for the problem, and the brackets represent the standard quantum mechanical commutation operation. For transport in one dimension, the density matrix in the coordinate representation, $\rho(x,x't)$, satisfies the equation of motion:

(2) $$i\hbar[\partial\rho(x,x',t)/\partial t + \{\partial\rho(x,x',t)/\partial t\}_{scattering}]$$

$$= -(\hbar^2/2m)[\partial^2/\partial x^2 - \partial^2/\partial x'^2]\rho(x,x',t) + [V(x,t)-V(x',t)]\rho(x,x',t)$$

The scattering operator is Hermetian and is represented in the proposed study phenomenologically, as discussed below. The expectation value of any operator A in the coordinate representation A(x',x) is:

(3) $$<A> = \int dxdx'\rho(x,x',t)A(x',x)$$

Note: if we erase all of the x' dependence in equation (2), including the spatial derivatives and the term V(x,t) we retrieve Schrodinger's equation. Thus there is an 'apparent' similarity. But the similarity ends here, for equation (2) states that a one dimensional physics problem requires a two dimensional differential equation. The origin of the second dimension lies in the fact that as in the Boltzmann transport equation in one dimension, transport requires both an incorporation of position and momentum. Scattering, of course, requires that momentum be treated as a three dimensional variable. In the discussion below, the transverse components of momentum are treated as separable variables except as they effect scattering. Two variables implies that the second variable is a transformed version of the momentum variable. In the calculations described the density matrix is solved simultaneously with Poisson's equation:

(4) $$\partial^2 V/\partial x^2 = -[e^2/\epsilon][\rho(x)-\rho_0(x)]$$

where $\rho(x)$ is the diagonal component of the density matrix and represents the density of carriers.

The density matrix is a 'matrix'. As is well known the elements of the matrix are dependent upon a 'basis'. Often the elements of the density matrix are classified in terms of quantum states. While in the discussion below we have chosen to deal with the density matrix in the 'coordinate' representation, this choice is not limiting in that a matrix transformation takes one matrix and transforms it into a mathematically equivalent matrix. The transformation results in an alternative physical description, but not new physics. The advantage of treating the density matrix in the coordinate representation is that the observables have a distinct **spatial and temporal evolution** that is not apparent from other descriptions.

While we will illustrate solutions to the equation of motion of the density matrix, we list the types of quantities that are required to describe quantum transport phenomena. We note that unlike the moment approaches to examining transport, these quantities are obtained **from** the density matrix. First there is the density of particles; which as discussed above is the diagonal element of the density matrix, $\rho(x,x)$. Second, there are the current density and energy density matricies. The diagonal components of the current density matrix are the position dependent expectation value of current; the diagonal components of the energy density matrix are the position dependent expectation values of energy. We list the three relevant quantities, all three of which contain real and imaginary components:

(5) density matrix: $\rho(x,x')$

current matrix: $j(x,x')$

energy matrix: $E(x,x')$

the time dependence is suppressed.

What does the density matrix look like? For free particles in the absence of any potential, and under time independent conditions, the density matrix (ignoring the exclusion principle) is given by:

(6) $$\rho(x,x') = \sum[\exp -E_i/k_bT]\Psi_i(x)\Psi_i^*(x')$$

The diagonal elements of equation (6) are given by

(6a) $$\rho(x,x) = \sum[\exp -E_i/k_bT]\Psi_i(x)\Psi_i^*(x)$$

and represent a Boltzmann distribution of particles. The diagonal elements of the density matrix **represent particle density.**

In identifying the other terms it has been deemed useful by Frensley (1990) and ourselves to introduce a coordinate transformation; this transformation simplifies the form of the equations and is extremely useful in highlighting the necessary computational requirements In performing these transformations we recognize that the second derivative operators in equation (2) can be expressed as follows:

(7) $$\partial^2/\partial x^2 - \partial^2/\partial x'^2 = [\partial/\partial x - \partial/\partial x'][\partial/\partial x + \partial/\partial' x]$$

Then with the transformation:

(8) $$\eta = (x+x')/2, \qquad \zeta = (x-x')/2$$

$$\partial/\partial\eta = \partial/\partial x + \partial/\partial x' \qquad \partial/\partial\zeta = \partial/\partial x - \partial/\partial x'$$

we find:

(9) $$\partial^2/\partial x^2 - \partial^2/\partial x'^2 = [\partial/\partial\zeta][\partial/\partial\eta]$$

In terms of the transformed variables the current density matrix (see also Iafrate et al, (1981) starting from a Wigner (1932) representation):

(10) $$j(x,x') = -(\hbar/2mi)[\partial\rho(x,x')/\partial x' - \partial\rho(x,x')/\partial x]$$

$$= (\hbar/2mi)\partial\rho(\eta+\zeta,\eta-\zeta)/\partial\zeta$$

It is important to note that evaluating the derivatives along the line $\zeta = 0$, yields the expectation value of current density. Note that since $\rho(x,x') = \mathrm{Re}\rho(x,x') + i\mathrm{Im}\rho(x,x')$, and $j(x,x') = \mathrm{Re}j(x,x') + \mathrm{Im}j(x,x')$, $\mathrm{Re}j(x,x')$ is obtained from $\mathrm{Im}\rho(x,x')$ and $\mathrm{Im}j(x,x')$ is

obtained from Reρ(x,x'). This is an extremely important result. Because we will assert that current transport through the device is represented by the diagonal elements of the real part of the current matrix j(x,x'). Thus if the density matrix is real the current is zero. The density matrix for free particles in the absence of any potential is real, thus the net current associated with a collection of free particles is zero. In terms of momentum states, this implies that for every quantum state with momentum **k** there is a quantum state with the opposite momentum -**k**.

It is worthwhile noting that with the definition of the current and density matricies we can write down a matrix continuity equation including off-diagonal elements:

$$(11) \qquad \partial\rho(\eta+\zeta,\eta-\zeta)/\partial t+\partial j(\eta+\zeta,\eta-\zeta)/\partial\eta$$

$$=(1/i\hbar)[V(\eta+\zeta)-V(\eta-\zeta)]\rho(\eta+\zeta,\eta-\zeta)$$

Along the diagonal, $\zeta=0$, and the real part of the above differential equation yields the 'familiar' continuity equation.

The energy matrix (see also Iafrate et al (1981)) is defined as:

$$(12) \qquad E(x,x')=-(\hbar^2/8m)[\partial^2\rho/\partial x^2-2\partial^2\rho/\partial x\partial x'+\partial^2\rho/\partial x'^2]$$

$$=-(\hbar^2/8m)\partial^2\rho/\partial\zeta^2$$

Again, evaluating the derivatives along the line $\zeta=0$, yields the expectation value of energy. Because the energy matrix is a new quantity we try to place this into the context of energy conservation. This is achieved by taking derivatives of the density matrix equation (2), with respect to ζ. We find, with $j(x,x')=p(x,x')/m$:

$$(13) \qquad \partial p(x,x')/\partial t+2\partial E(x,x')/\partial\eta =$$

$$-(1/2)\partial[V(x)-V(x')]/\partial\zeta\,\rho(x,x')-(1/2)[V(x)-V(x')]\partial\rho(x,x')/\partial\zeta$$

Now, $\partial/\partial\zeta[V(\eta+\zeta)-V(\eta-\zeta)]=[V'(\eta+\zeta)+V'(\eta-\zeta)]$, where the prime denotes derivative with respect to the argument of the respective functions. Thus along the diagonal:

$$(14) \qquad \partial p(x,x)/\partial t+2\partial E(x,x)/\partial\eta=-\partial[V(x)]/\partial\eta\,\rho(x,x)$$

Since p(x,x') and E(x,x') are density dependent quantities, equation (13) is Newton's Law for momentum density.

The above description is an indication of the types of terms to be evaluated in the density matrix.

3. Results

3a. Steady State Results

The calculations that follow are for GaAs/AlGaAs RTD in which the GaAs quantum well is

50Å wide. The AlGaAs barriers are either 50Å wide, or in one case, to compare with the experimental results of Eaves and co-workers (1989) include an asymmetric 100Å barrier. The time independent GaAs/AlGaAs calculations fall into four categories:

(1) Figures 2 and 3; 1500Å structure, with successively
(i) GaAs, 625Å, $10^{18}/cm^3$,
(ii) GaAs, 50Å, $10^{15}/cm^3$,
(iii) AlGaAs, 50Å, $10^{15}/cm^3$, barrier 300 mev
(iv) GaAs, 50Å, $10^{15}/cm^3$,
(v) AlGaAs, 50Å, $10^{15}/cm^3$, barrier 300 mev
(vi) GaAs, 50Å, $10^{15}/cm^3$,
(vii) GaAs, 625Å, $10^{18}/cm^3$,

(2) Figures 4, 5 and 6; 1500Å structure, with successively
(i) GaAs, 475Å, $10^{18}/cm^3$,
(ii) GaAs, 200Å, $10^{15}/cm^3$,
(iii) AlGaAs, 50Å, $10^{15}/cm^3$, barrier 300 mev
(iv) GaAs, 50Å, $10^{15}/cm^3$,
(v) AlGaAs, 50Å, $10^{15}/cm^3$, barrier 300 mev
(vi) GaAs, 200Å, $10^{15}/cm^3$,
(vii) GaAs, 625Å, $10^{18}/cm^3$,

(3) Figure 7; 1500Å structure, with successively
(i) GaAs, 400Å, $10^{18}/cm^3$,
(ii) GaAs, 200Å, $10^{15}/cm^3$,
(iii) AlGaAs, 50Å, $10^{15}/cm^3$, barrier 300 mev
(iv) GaAs, 50Å, $10^{15}/cm^3$,
(v) AlGaAs, 10Å, $10^{15}/cm^3$, barrier 300 mev
(vi) GaAs, 200Å, $10^{15}/cm^3$,
(vii) GaAs, 500Å, $10^{18}/cm^3$,

(4) Figure 8; 1500Å structure, with successively
(i) GaAs, 425Å, $10^{18}/cm^3$,
(ii) GaAs, 200Å, $10^{15}/cm^3$,
(iii) AlGaAs, 100Å, $10^{15}/cm^3$, barrier 300 mev
(iv) GaAs, 50Å, $10^{15}/cm^3$,
(v) AlGaAs, 50Å, $10^{15}/cm^3$, barrier 300 mev
(vi) GaAs, 200Å, $10^{15}/cm^3$,
(vii) GaAs, 475Å, $10^{18}/cm^3$,

Figure 2 displays the potential, the density distribution and a term referred to as the quantum potential, discussed below. These calculations are performed for bias levels prior to the peak current value in the RTD. The peak current is assumed to occur when the quasi-bound state in the quantum well reaches a characteristic energy state near the edge of the accumulation layer. For these calculations it is assumed that the quasi-Fermi level of the emitter and the quasi-Fermi level of the quantum well are at the same value. This value

of the quasi-Fermi level is based upon an assumption as to what the distribution function should be within the quantum well. The quasi-Fermi level of the collector barrier is assumed to linearly decrease until the end of the collector barrier, at which point it is equal to that of the collector contact. The calculation reveals that the charge in the quantum well increases with increasing bias as suggested by Ricco and Azbel (1984), and as has been seen experimentally (Eaves and co-workers (1989)). Note that as the bias is increased, the increasing charge in the well is accompanied by an increasing potential energy drop across both the emitter and collector barriers, but that the largest potential drop is across the collector barrier. The presence of charge within the quantum well screens the emitter barrier as discussed by Eaves and workers (1989) and only small emitter changes accompany the bias changes. As indicated by the arrows, the density of carriers in the quantum well increases, the density of carriers in the accumulation layer increases and the density of carriers in the collector region decreases. The net charge density is unchanged.

For diagnostic purposes we have introduced the quantum potential:

$$(15) \qquad Q = -[\hbar^2/2m][\partial^2 \sqrt{\rho}/\partial x^2]/\sqrt{\rho}$$

which represents the real part of the energy operator in Schrodinger's equation. We find that $Q + V(x)$, yield an approximate representation of the energy of the quasi-bound state within the quantum well. In figure 2 we display the term $Q + V$, and note that it decreases with increasing collector bias. Near V_p, $Q + V$ in the quantum well is approximately equal to $Q + V$ in the accumulation region.

The situation in figure 3 corresponds to the case in which there is a current drop. Note for this calculation it was assumed that once the electron density within the quantum well exceeded a value of $10^{12}/cm^2$, that there would be strong carrier scattering. As discussed by Eaves et al (1989), a new quasi fermi level forms that is different from that of the emitter. For the calculation the quasi-Fermi level was taken to vary linearly from its value at the emitter barrier to its value at the collector barrier. We note here that for this case, that the charge in the well has disappeared. This removes the screening of the emitter barrier which can now be lowered, there is an increase in charge upstream of the emitter, and the sum of $Q + V$ is no longer constant, indicating that the tunneling process is no longer one of resonant tunneling.

The above calculations were repeated for the situation in which there were 200Å spacer layers on either side. The reason for this calculation was that there was experiment (Ray et al.(1986)) to which comparison could be made. These experiments were for 500Å space layers and some adjusting was necessary. The space charge calculations are displayed in figures 4 and 5, and the comments made in connection to those associated with figures 2 and 3 are applicable here. The interesting feature is the close agreement of the peak to valley ratios with experiment as shown in figure 6. This point should not be underestimated in that virtually all previous calculations with the exceptions of several Wigner function calculations have led to peak to valley ratios that are orders of magnitude in excess of those seen experimentally.

To summarize the significance of Figures 2 through 6, we note that for voltages to V_p transport across the quantum well is approximately Fabry-Perot coherent scattering.

Beyond V_p a significant contribution from incoherent scattering is required to lower the emitter barrier with the consequent drop in current.

The situation discussed above is present in the case of asymmetric structures of the type discussed by Eaves and co-workers (1989), but there are several interesting features that should be noted. As displayed in figures 7 and 8 for the case when the wide barrier is at the collector side there is a gradual buildup of charge in the quantum well, with features very similar to those of figures 4 and 5. For the case where the wide barrier is at the emitter, there is a larger potential drop across the emitter barrier with a consequent lowering of the bottom of the conduction band below that when the wide barrier is at the collector. The result is a rapid increase with bias of charge within the quantum well. It is anticipated that the peak current will occur for lower values of V_p, when the thin barrier is the collector. This is confirmed by Eaves (1991).

3b. Time Dependent Results

Time dependent calculations were initiated to determine the characteristics of the filling and emptying of the quantum well. As discussed above the filling and/or emptying of the quantum well occurs at a fixed value of applied bias and occurs after of thermalization processes. These calculations were performed in which (a) initially the well is empty, figure 9; and (b) initially the well was filled, figure 10. The calculations are for the structure of Figures 2 and 3, at -200 mev, but with the heavily doped regions reduced from 625Å to 475Å. Since the potential drop across these regions is small the alterations in the results from reducing the device length is expected to be negligible.

Figure 9 displays a sequence of calculations in which the quantum well is being filled. The equilibrium distribution as well as the initial charge distribution within the well are indicated. Under equilibrium conditions there is charge in the quantum well. The equilibrium distribution represents the zero applied bias case. The initial distribution is under bias and displays charge accumulation on the emitter side but no charge in the quantum well. The transient filling of the well occurs as a result of the anticipated cooling of the electrons as the voltage decreases across the barriers. While this occurs at a fixed external bias, the device is connected to the external bias through a resistor, and as the current across the resistor increases the voltage across the double barriers decreases. This change is accomplished numerically by altering the quasi-fermi level within the double barrier region, from varying linearly across the well, to a value that is constant across the well.

Figures 9(b) through 9(f) display calculations showing the progressive filling of the quantum well. The initial state is represented in figure 9a with accumulation on the emitter order, and zero charge in the quantum well. The final state is that of figure 10a. Frame 9b through 9f include all previous time sequences, and thus represent overlays. The oscillations in density represent incident and reflected space charge contributions. At 50fs, approximately 10% of the maximum space charge has entered the well suggesting a switching time of 500fs.

Figure 10 displays a sequence of calculations in which the quantum well is being emptied. The initial distribution is under bias and displays charge in the well. The final distributions is represented by figure 9a. The transient emptying occurs as a result of an anticipated

heating of the carriers as the voltage across the barriers increases. While this occurs at a fixed external bias, the device is connected to the external bias through a resistor, and as the current across the resistor decreases, the voltage across the double barrier diode increases. This change is accomplished numerically by altering the quasi-fermi within the double barrier region, from a constant across the quantum well to one that varies linearly downward across the quantum well. As in figure 9, each frame includes all previous time sequences. At 10fs, approximately 2% of the charge has been removed suggesting a switching time of 500fs.

Figure 11 displays a sequence of time plots to determine the time dependent response of a filled quantum well to a sinusoidal time dependent change in potential 200 (mev) + 10(mev) sinωt. The presence of the charge in the well prevents the structure from following the time dependent variation of potential. Figure 12 displays a sequence of time plots to develop the time dependent response of an empty quantum well to a time dependent change in potential. Both figures 11 and 12 are for a frequency of 10^{14} radians/sec. The absence of charge in the well permits the structure to follow the time dependent change in bias.

Figure 13 and 14 displays the results of a time dependent calculation for a structure nominally similar to that of figure 11. There are differences. Figures 13 and 14 include a barrier height of 350 mev. For this case we estimate a second quasi-bound state near 300 mev. The quantum well was probed at frequencies near the estimated frequency difference between the ground state at the first excited state. The results are qualitatively similar to that of figure 11, and demonstrate that the response of the system is dependent upon the fact that the carriers do not respond instantaneously to an imposed excitations. This last feature suggests that the primary means of determining the response of the RTD to external sources is to simulate the operation of the device in an environment close to that in which it will be operated.

It should be noted, however, that part of the motivation for choosing frequencies corresponding to the energy difference of the quasi-bound ground state and the first excited state was to determine if the quantum well could be viewed as an "atom". The initial calculations suggest that the presence of space charge tends to prevent this. But the absence of systematic frequency tuning prevents us from making an unequivocal statement.

3c. Material Dependence

An issue that has surfaced in the studies of the RTD is the role of material properties. The studies of Reed et al. (1986) with an InGaAs quantum well suggest a strong material dependence, and indeed this is observed. Figures 15 and 16 display calculations for a structure similar to that of figures 2 and 3, but with one significant exception: the center of the quantum well, over a distance of 30A is lowered in energy by 100 mev with the device structure reduced to 1200Å. While this is not InGaAs the trend is toward InGaAs. First note, that even though the quantum well is narrower than that of figure 2, there is considerably more change in the quantum well. Note also the apparent absence of emitter accumulated charge, and to consequent upward slope of the potential across the emitter barrier. For voltages above V_p, there is a reduction of charge in the well, but for the same linearly varying quasi-fermi level as in figure 3, the charge reduction is mitigated. Indeed if

we compare the bottom of the conduction band in figure 2 and 16, it is seen that the carriers have a longer tunneling region to traverse toward the collector contact.

4. Future Research

The Phase I program identified four broad areas of interest of study. It is recommended that further studies attempt to design structures that exploit these characteristics of RTDs. The first issue is how high in frequency can these structures be electrically operated. The second issue is the switching speed of the RTD. The third issue concerns the power levels of RTD's. The fourth issue involves material properties. We examine each issue separately.

4a. Frequency Issues

The Esaki tunnel diode, the Gunn diode and others are capable of being operated as self-excited oscillators. In this configuration, as represented in figure 17, the RTD which when undergoing self-excited oscillations has an equivalent circuit schematically represented by inset (a) in figure 17, which shows a dc negative differential resistor in parallel with a voltage dependent capacitor. When the device is not operating as a self excited oscillator, the equivalent circuit is more like that of inset (b) where the resistor is a saturated current resistor.

When does one equivalent circuit enter the picture and the second leave the picture? The principal investigator has discussed this most recently with respect to transferred electron Gunn oscillators. In that case it was determined that apart from circuit parameters, negative differential resistance disappeared at frequencies in excess of the time it took for carriers to transfer from the Γ to the L valley in GaAs.

For the resonant tunneling picture we are not specifically concerned with k space transfer, but instead the response time of the charge density waves within the quantum well. As figures 11 through 15 show the response time is dependent upon the amount of charge in the well. It is anticipated that at sufficiently high frequencies negative differential conductivity will disappear. This will be the upper frequency limit for RTD's. Thus one new task should be undertaken to determine the upper frequency limit of the RTD when used as a local oscillator in a self-excited oscillating circuit. If self-excited oscillators at terahertz frequencies can be achieved, then structures for reasonable power levels will be considered. To deal with this task the equation of motion of the density matrix, and Poissons equation must be coupled to an ordinary differential equation representation of the circuit of figure 17:

$$(16)\quad V_{bias} = V_{rtd} + IR + LdI/dt$$

4b: Speed Issues

The calculations of figures 9 and 10 display the time dependent filling and emptying of the quantum well. The results of the calculation stress that the resonant tunneling structure is controlled by the amount of charge in the quantum well. If this is the case, then the situation envisioned in figure 18 should be possible. In figure 18 we sketch the dc current voltage characteristics of a resonant tunneling structure biased just below threshold. We

illuminate the structure with light whose wavelength is such as to permit generation of excess electron-hole pairs in the quantum well. While we have not examined the distributions of holes in such a structure the excess distribution of electrons should result in the charge rearrangement described in figures 9 and 10 and provide a means of switching to the state B described in figure 18. Further the results suggest that if the bias point was at the lower A' point, that with increased illumination switching would also occur.

The above concepts have been demonstrated by England, et al. (1991). For an AlGaAs/GaAs RTD with the current voltage characteristics displayed in figure 18b, optical switching was observed. Under zero illumination, the experiments indicated switching at 0.692V. Close to the intrinsic switching point only 10μW of power was needed to switch. However as the voltage is moved further from the switching a near exponential increase in power is required to switch the device. The tentative explanation of England et al (1991) is consistent with our discussion and is related to the charge rearrangement within the RTD. England et al (1991) argue that the switching offers the possibility of controlling substantial current changes with small optical signals, i.e., the development of an "optical thyristor". The advantage of using an RTD as a switch is that the structure remains in the switched or unswitched mode while electrical power is applied. In this respect, as discussed by England et al (1991), it can operate as a static optical memory.

It is recommended that the RTD be studied as an optical switch. Several components are needed. First, an equation similar to that of equation (2) will be included for holes. The coupling of electrons and holes through the Liouville equation is part of SRA's ongoing program. Second, an equation for generating excess electron-hole pairs must be introduced. SRA has experience in this area. Third, the presence of traps modifies all of the relevant equations. In Poisson's equation the background density is replaced by an expression for the net background charge density

$$\rho_0 \Rightarrow (N^+ - P^-) \tag{17}$$

which represents the net background density. (Poisson's equation will also include holes.) If N and P denote the net numbers of donor and acceptor impurities including ionized and neutral (denoted by the subscript 'o')

$$\begin{aligned} N &= N^+ + N_0 \\ P &= P^- + P_0 \end{aligned} \tag{18}$$

The scattering term in equation (2) includes a term representing generation and recombination, R_n, which for a single set of donor trap levels is represented by the following equation:

$$R_n = C_n^+ [\rho_d N_0 - \rho N^+] \tag{19}$$

The coefficients C_n^+, ρ_d, represent capture cross sections and equilibrium concentration values.

Thus new work is recommended that will involve coupling the density matrix equation for electrons and holes with Poissons equations, a simple resistive circuit, and the rate equations for the carrier trapping to examine the RTD as an optical switching element.

4c. Power Level Issues

One issue with resonant tunnelling structures has been the power levels. Recent experiments by Dellow et al (1991) suggest a means of addressing this. For vertical FET structures shown in figure 19 they demonstrated gated control of resonant tunneling. This structure immediately suggests the fabrication of PBT-like structures in which the base surrounds the RTD, as shown in figure 19c. Figure 19c displays one cell of a permeable base transistor. Clearly, if this could be fabricated satisfactorily high frequency current levels could be achieved. The study would involve the design of the RTD/PBT. This is a two dimensional program, these results of which require implementation of a two dimensional algorithm. Such an algorithm is already under development under a concurrent AFOSR program. It is worthwhile recognizing that while the PBT is apparently difficult to fabricate, the advantage for phase coupling of multiple RTDs in a PBT configuration may provide compelling reasons to reconsider the PBT for possible near terahertz operation.

5. Conclusions

The Liouville equation of motion for the density matrix has been solved numerically to obtain time-independent and time-dependent characteristics of RTD's. Time-independent solutions show that as the bias is increased the density of carriers in the quantum well increases, the density of carriers in the accumulation layer increases and the density of carriers in the collector region decreases. The increasing charge in the well is accompanied by an increasing potential drop across both the emitter and collector barriers, but the largest potential drop is across the collector barrier. For these calculations it is assumed that the quasi-fermi level of the emitter and the quasi-fermi level of the quantum well are at the same value. Beyond the peak current, the quasi-fermi level was assumed to vary linearly from its value at the emitter barrier to its value at the collector barrier. In this case the charge in the well has disappeared. Peak to valley ratios of the computations are in close agreement with experiment. Computations carried out to simulate an InGaAs quantum well show a strong material dependence of RTD characteristics.

Time dependent computations carried out for a RTD indicate that a characteristic time scale for such a device is the time required to fill or empty the quantum well. This time scale was estimated to be about 500 fs for the RTD considered here. Computations of the response of the RTD to a sinusoidal time-dependent potential suggest that the space charge in the quantum well prevents the well from being viewed as an "atom" when probed at frequencies corresponding to the energy difference of the quasi-bound ground state and the first excited state.

6. Acknowledgement

We would like to acknowledge help from Beverly Morrison during the course of this study.

References

M. W. Dellow, P. H. Beton, M. Henini, P. C. Main, L. Eaves, S. P. Beaumont and C. D. W. Wilkinson, Elec. Letts. 27, 134 (1991).
L. Eaves, Private Communication (1991).
L. Eaves, M. L. Leadbeater, D.G. Hayes, E.S. Alves, F.W. Sheard, G.A. Toombs, P.E. Simmonds, M.S. Skolnick, M. Henini, and O. H.Hughes, Solid State Electronics 32, 1101 (1989).
P. England, J. E. Golub, L. T. Florez and J. P. Harbison, Appl. Phys. Letts. 58, 887 (1991).
W. R. Frensley, J. Vac. Sci. Technol, B3, 1261 (1985).
W. R. Frensley, Phys. Rev. B36, 1570 (1987)
W. R. Frensley, Rev. Mod. Phys. 62, 745 (1990)
G.J. Iafrate, Closing remarks at the Hot Carrier Conference , Tempe (1989)
G. J. Iafrate, H. L. Grubin and D. K. Ferry, J. dePhysique C7,227 (1981)
A. M. Kriman, N. C. Kluksdahl and D. K. Ferry Phys. Rev. B 36, 5953 (1987)
S. Ray, P. Ruden, V. Sokolov, R. Kolbas, T. Boonstra and J. Williams, Appl. Phys. Letts., 48, 1666 (1986).
M. A. Reed, R. J. Koestner and M. W. Goodwin, Appl. Phys. Letts. 22, 562, (1986).
B. Ricco, and M. Y. Azbel, Phys. Rev B29, 1970 (1984)
E. D. Wigner, Phys. Rev. 40, 749 (1932).

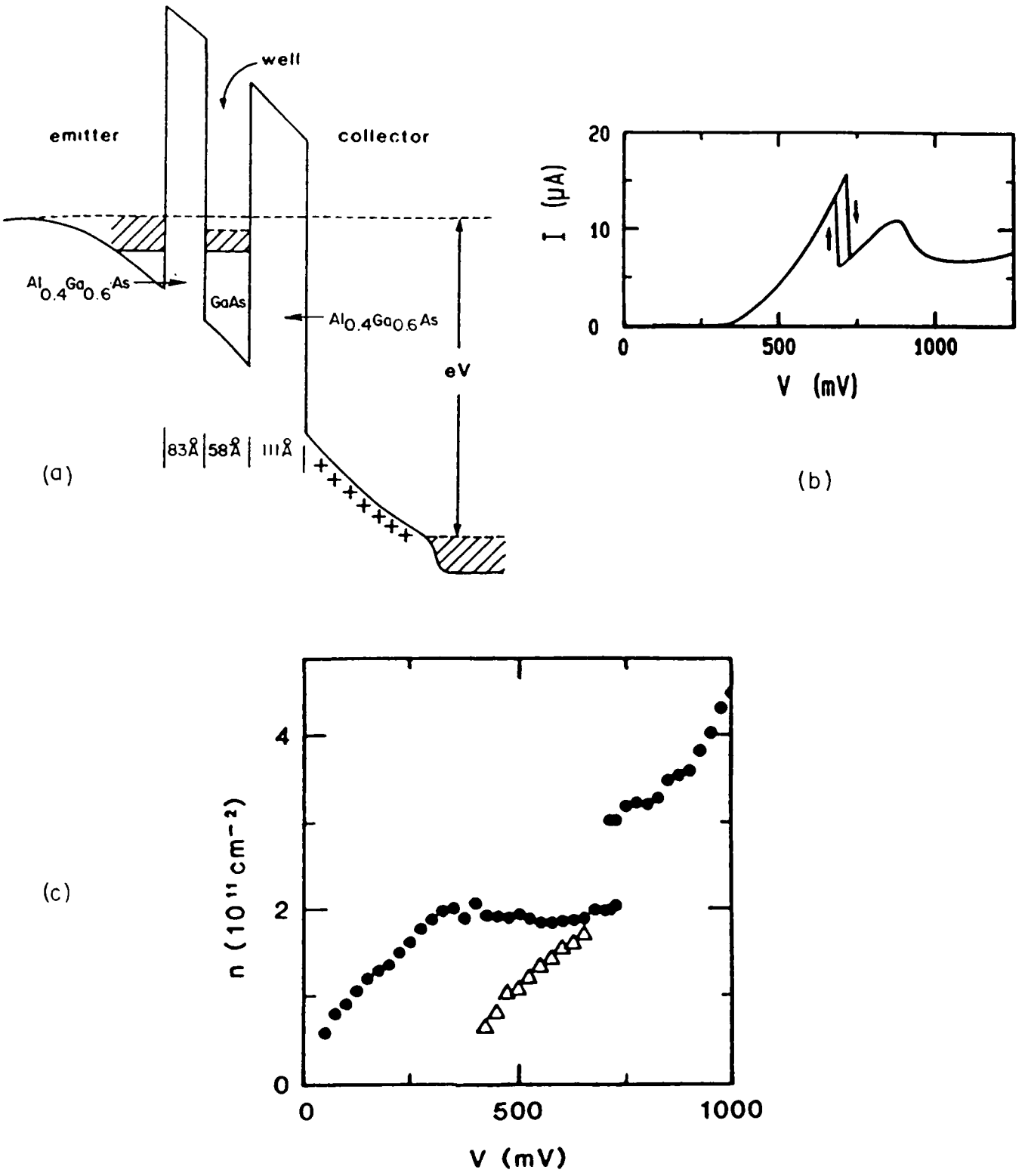

Figure 1. (a) Conduction band schematic under applied voltage showing bound state levels (solid lines) and quasi-fermi levels (-lines). (b) DC current voltage characteristics at 4K. (c) Areal density vs. voltage for charge in emitter accumulation layer (circles) and quantum well (triangles). From Eaves and co-workers (1989).

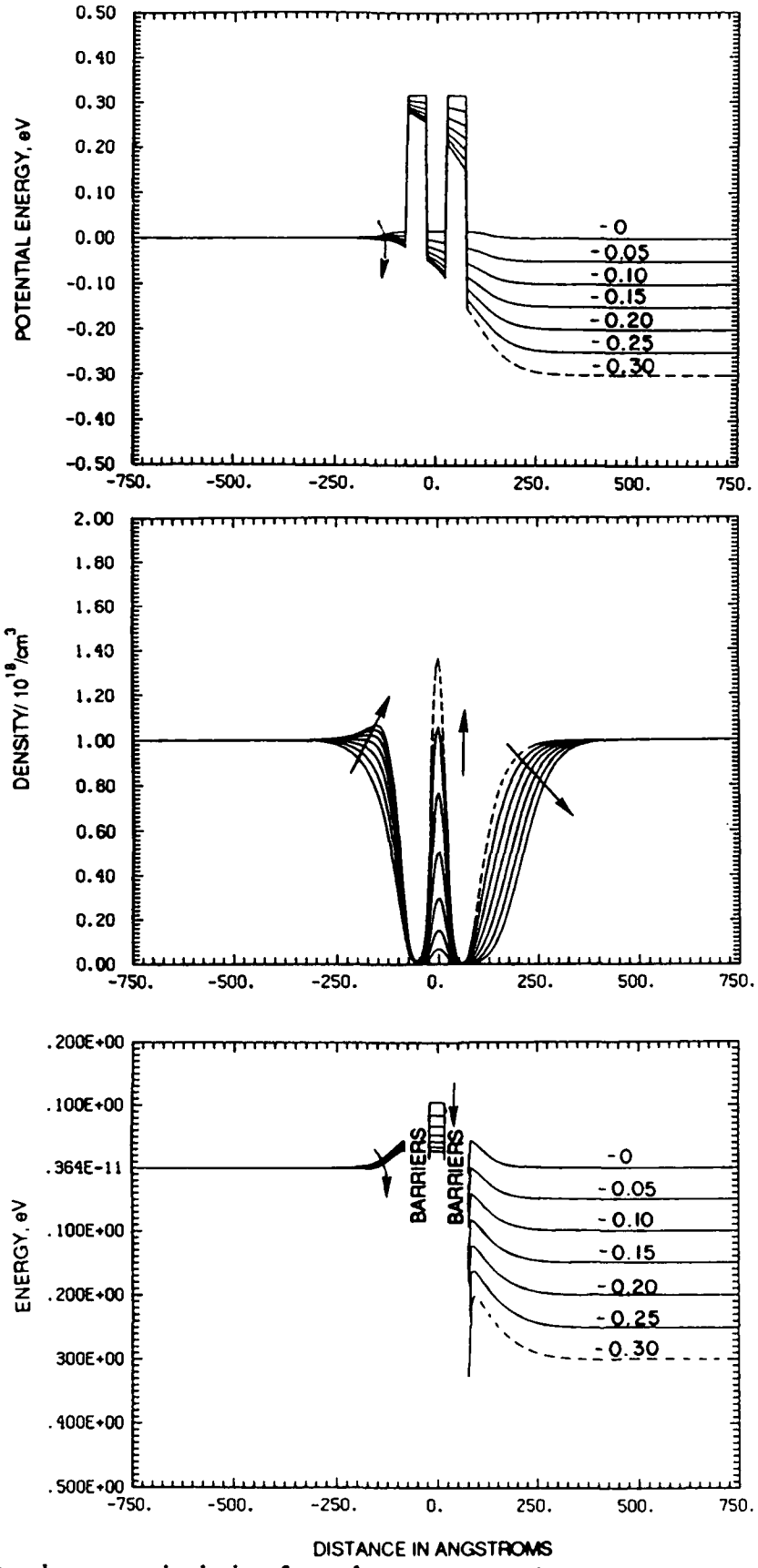

Figure 2. Steady state calculation for voltages to an estimated V_p, the voltage at peak current. (a) Potential energy vs. bias. Arrow points in direction of increasing collector bias. (b) Density vs. bias. Arrows point in direction of charge variation with increasing bias. (c) Quantum potential plus potential energy. Arrows point in direction of variation with increased bias.

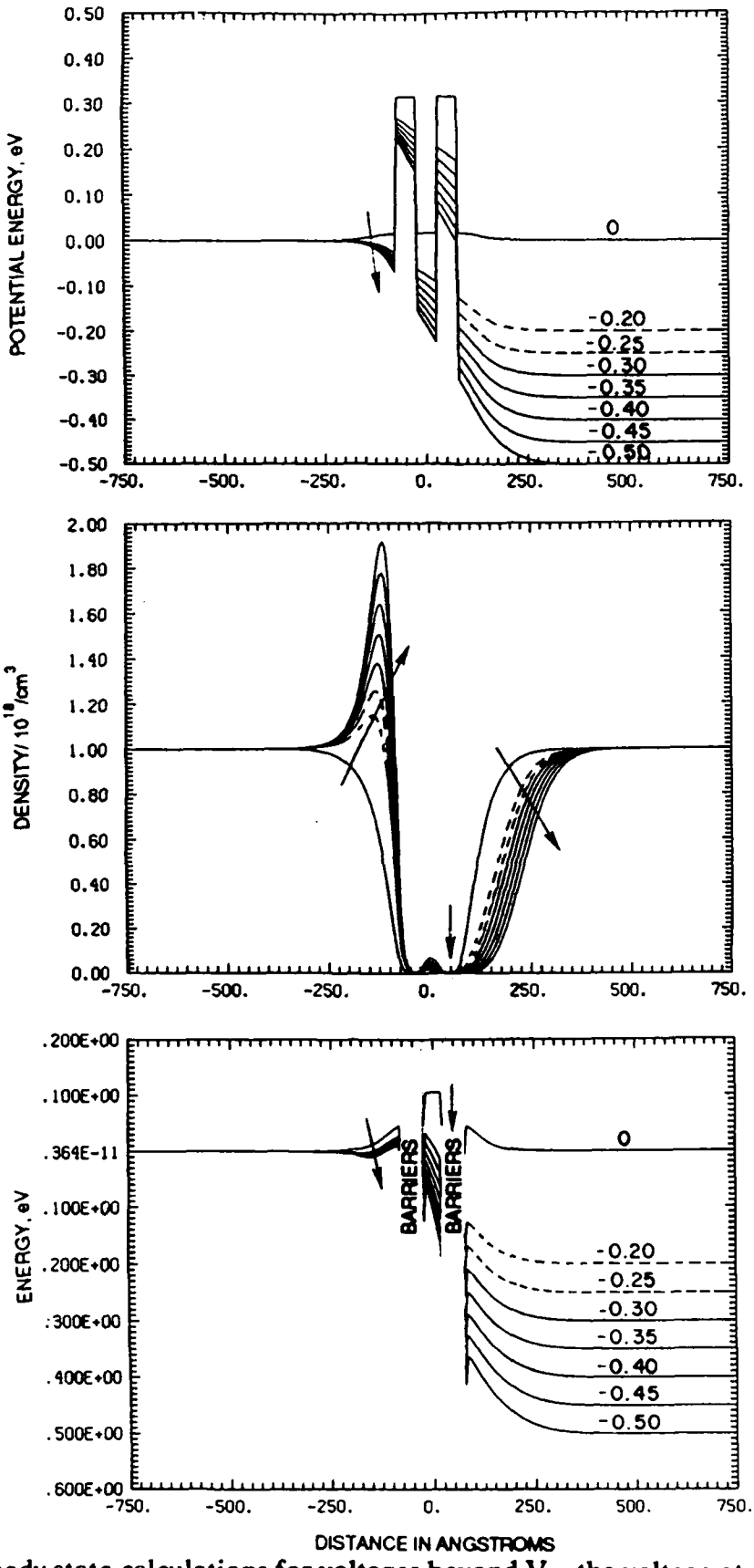

Figure 3. Steady state calculations for voltages beyond V_p, the voltage at peak current. (a) Potential energy vs. bias. Arrow points in direction of increasing collector bias. (b) Density vs. bias. Arrows point in direction of charge variation with increasing bias. (c) Quantum potential plus potential energy. Arrows point in direction of variation with increased bias.

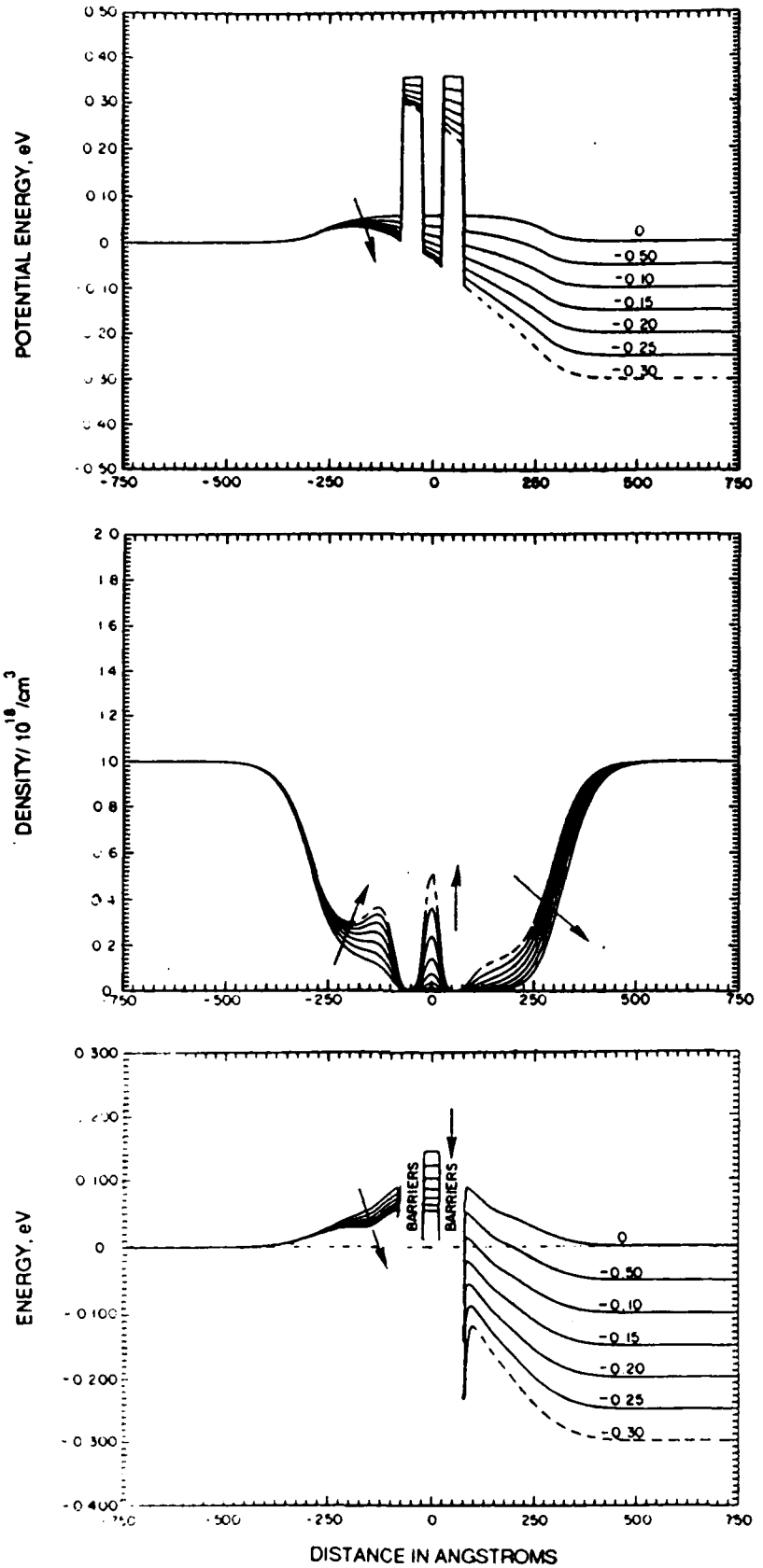

Figure 4. Steady state calculation for voltages to an estimated V_p, the voltage at peak current. (a) Potential energy vs. bias. Arrow points in direction of increasing collector bias. (b) Density vs. bias. Arrows point in direction of charge variation with increasing bias. (c) Quantum potential plus potential energy. Arrows point in direction of variation with increased bias.

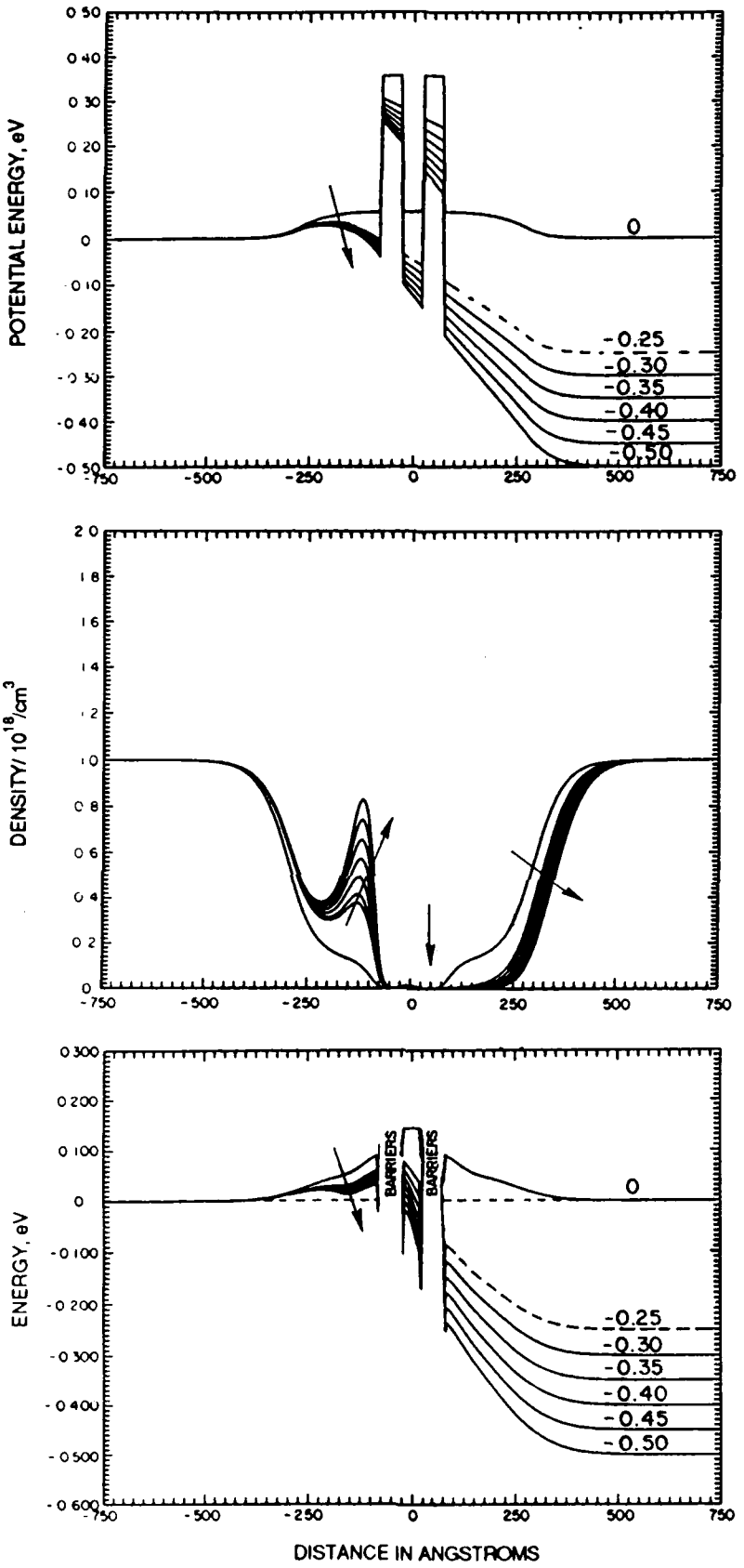

Figure 5. Steady state calculations for voltages beyond V_p, the voltage at peak current. (a) Potential energy vs. bias. Arrow points in direction of increasing collector bias. (b) Density vs. bias. Arrows point in direction of charge variation with increasing bias. (c) Quantum potential plus potential energy. Arrows point in direction of variation with increased bias.

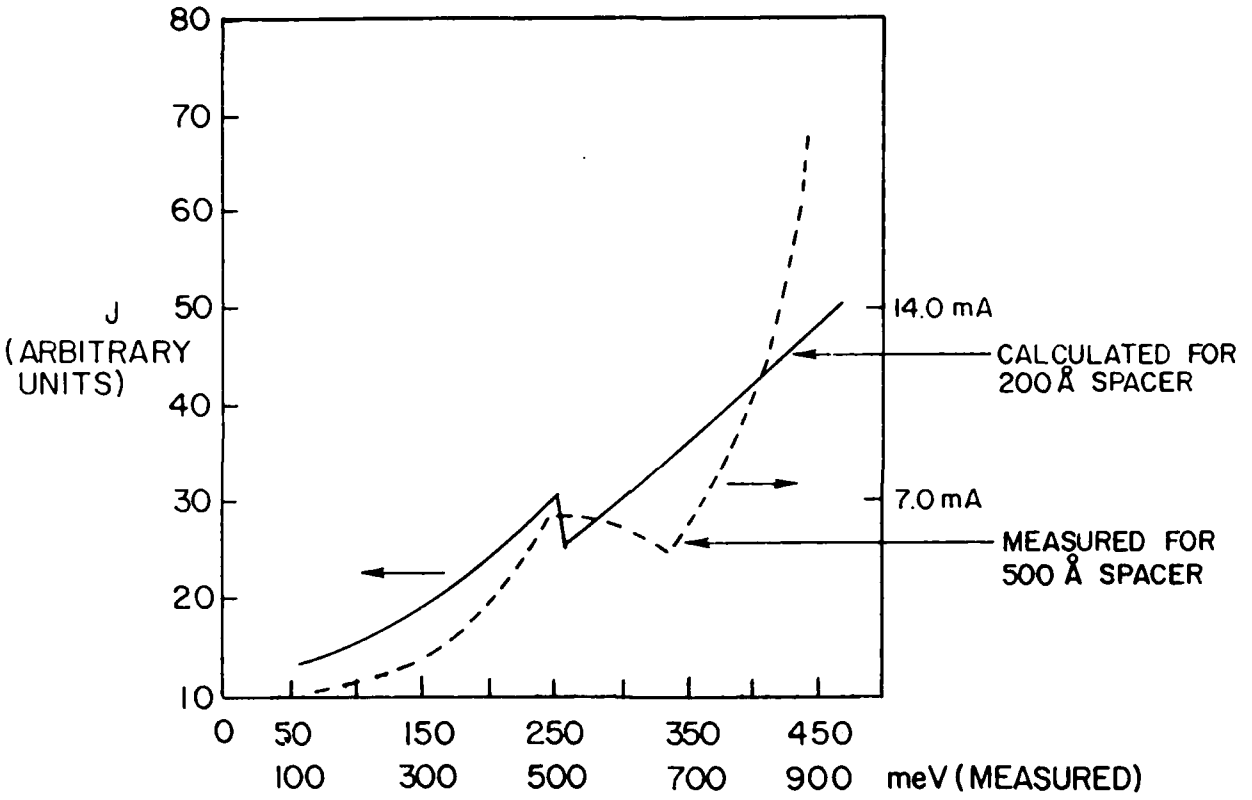

Figure 6. Current vs. voltage for structure of figures 4 and 5. Measured values are from Ray et al. (1986). The calculated current values are in arbitrary units and are scaled to the measured values. Because the calculations were for smaller structures with 200Å spacer layers, as against the measured 500Å structures, the peak current was measured at higher voltages.

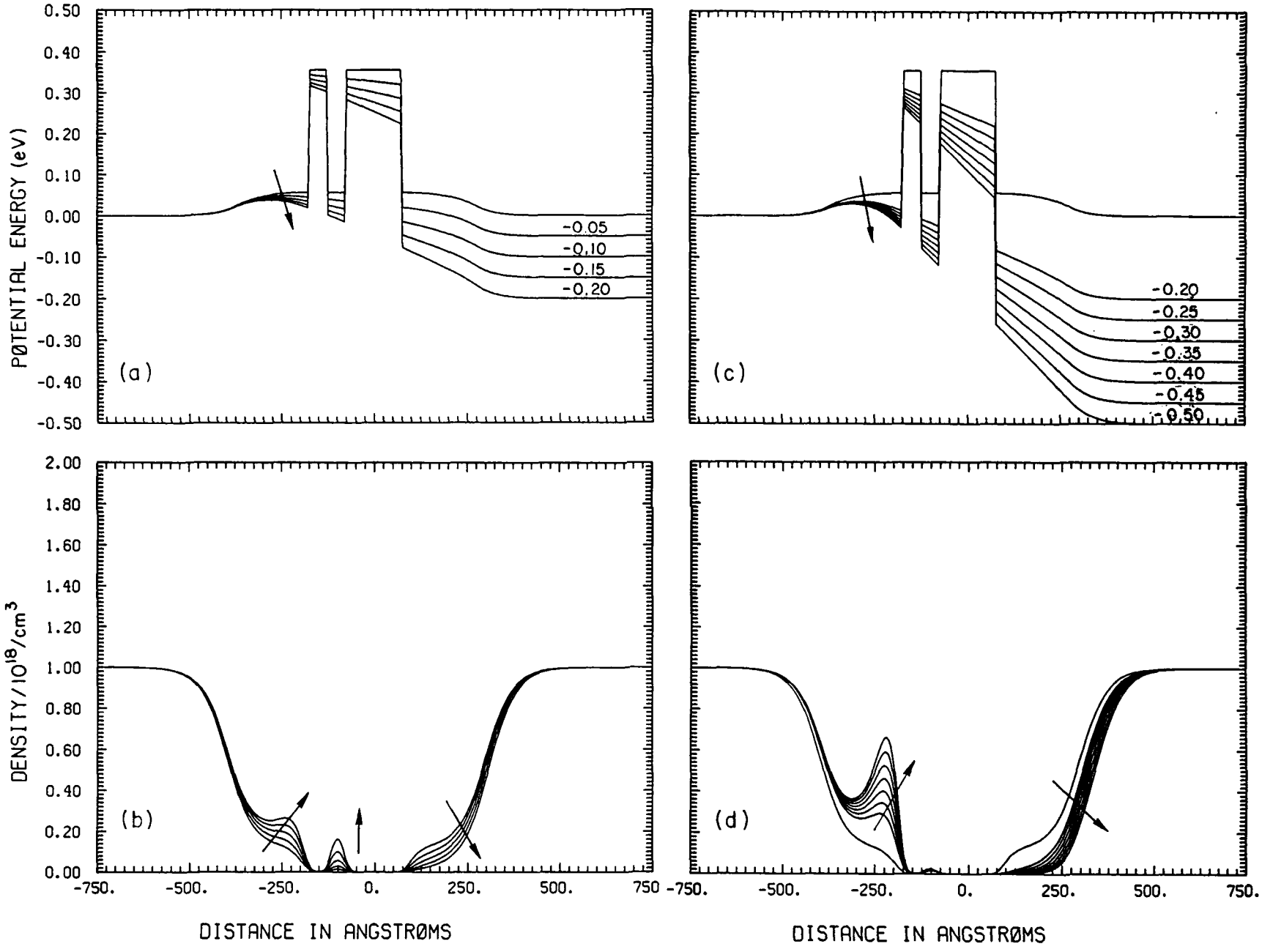

Figure 7. (a and b) Steady state calculations for voltages to an estimated, V_p, the voltage at peak current. (c and d) Steady state calculations for voltages beyond V_p. Arrows denote direction of change with increasing collector bias.

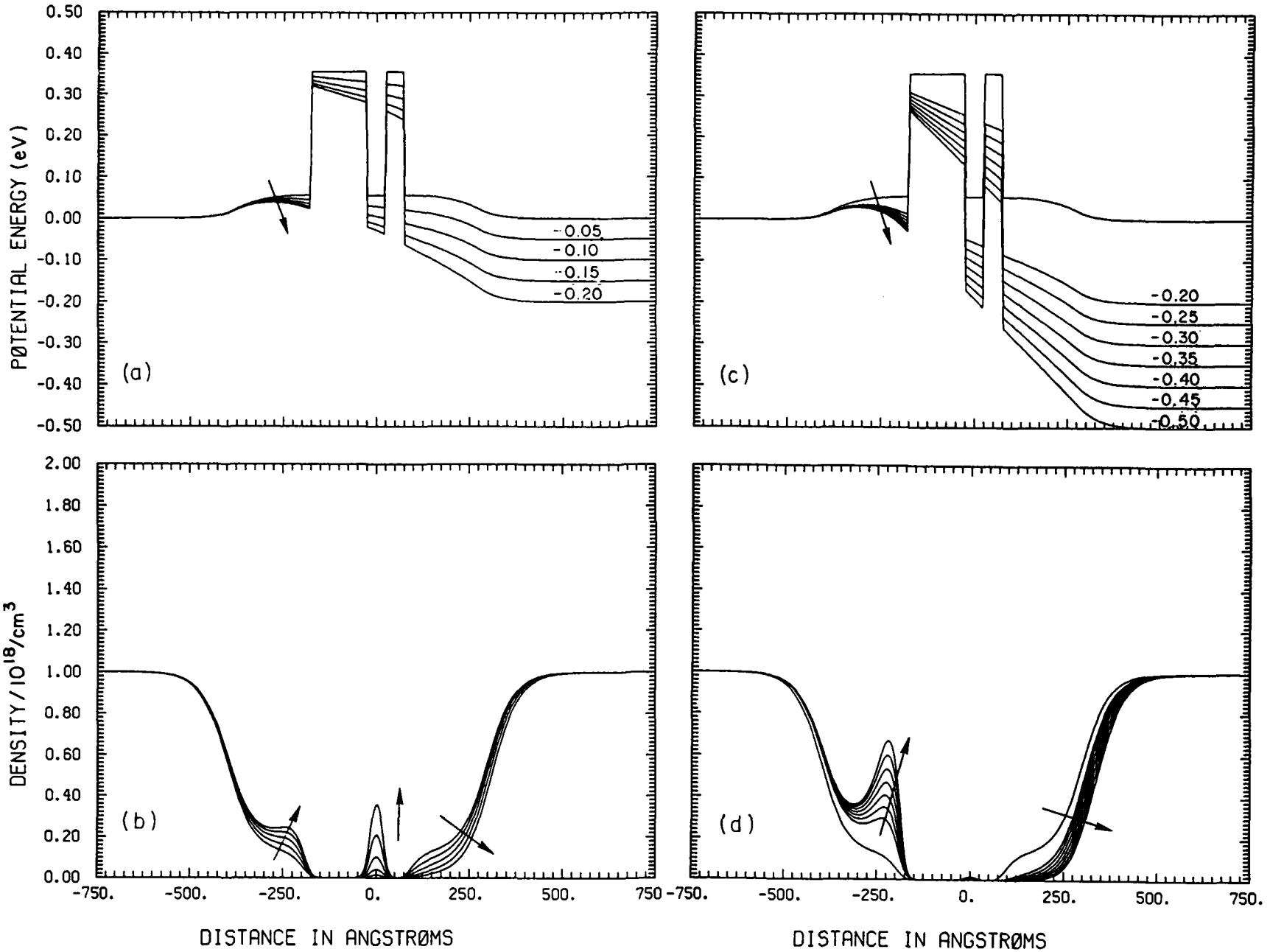

Figure 8. (a and b) Steady state calculations for voltages to an estimated, V_p, the voltage at peak current. (c and d) Steady state calculations for voltages beyond V_p. Arrows denote direction of change with increasing collector bias.

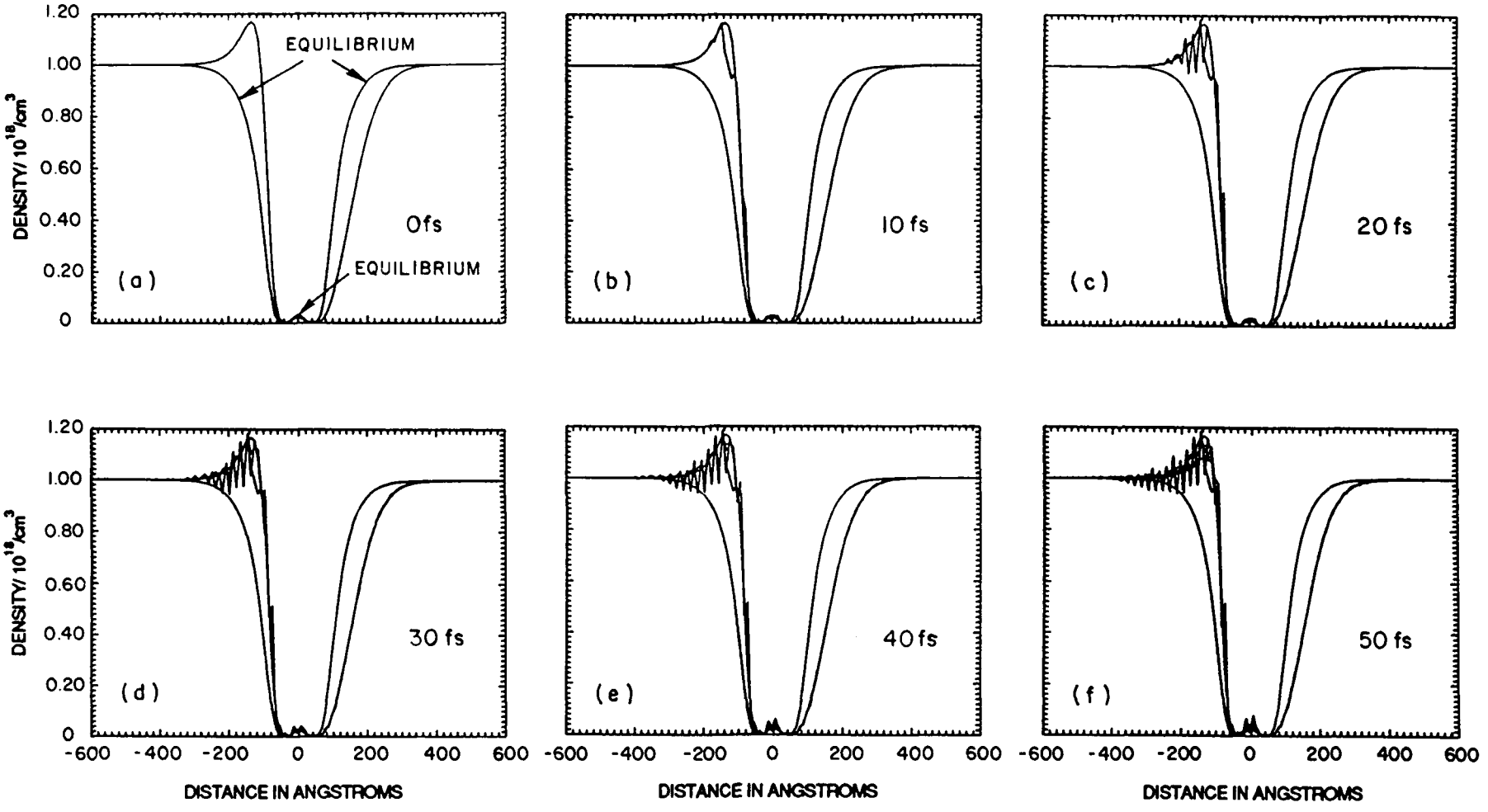

Figure 9. Time sequence in filling the quantum well. (a) Density distribution is a steady state one for a quasi-fermi level varying linearly from emitter to collector barrier. Density distribution is not in steady state when quasi-fermi level is constant across quantum well. In the latter, the steady state has significance charge in the well as shown in figure 10a. Figures (b) through (f) showed temporal evolution through first 50 fs. Note: Each figure incorporates the temporal evolution of proceeding figures thus f includes overlays of (a) through (e). The final state is that of figure of 10a.

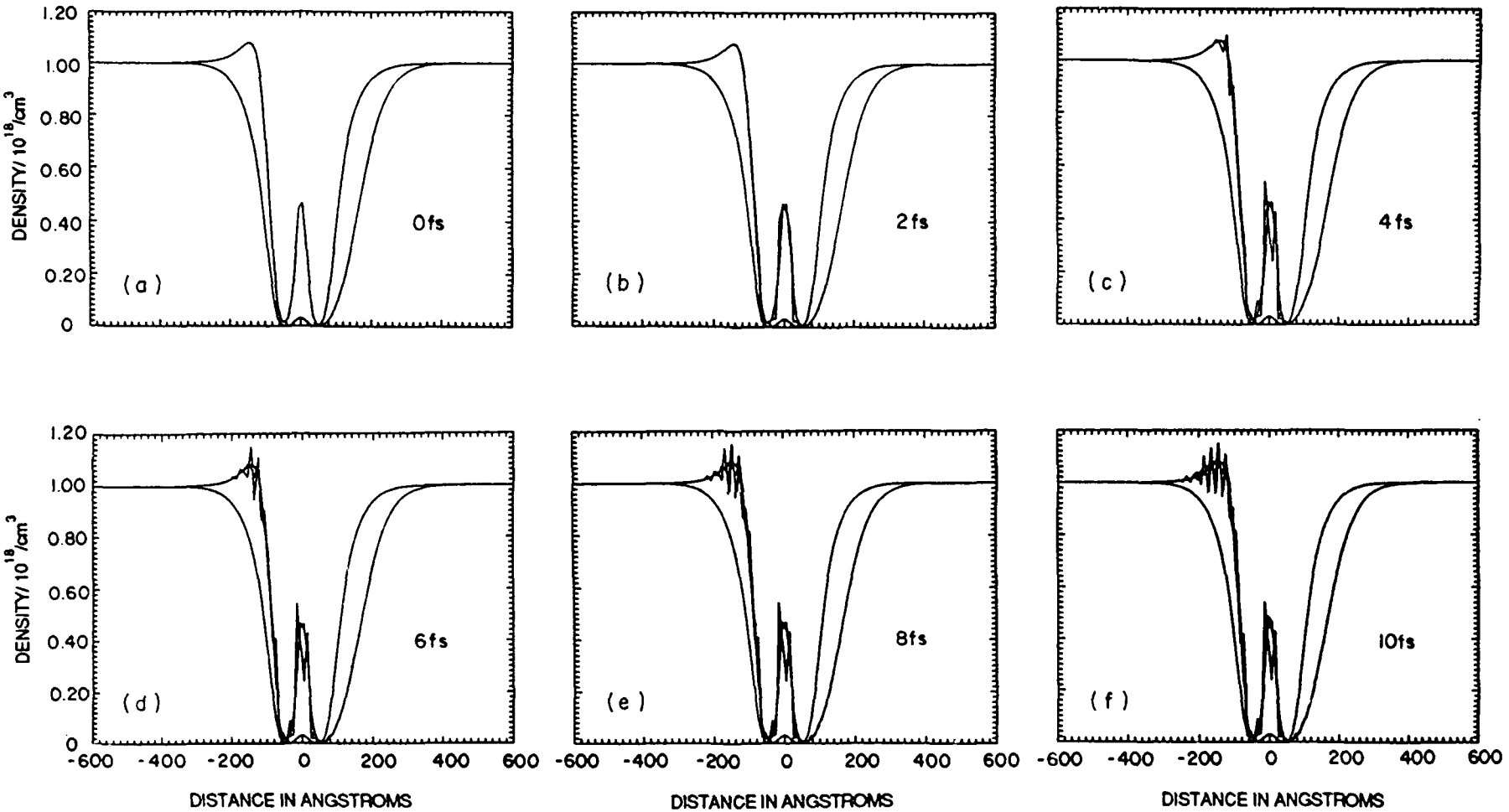

Figure 10. Time sequence of emptying the quantum well (a) Density distribution is a steady state and for a quasi-fermi level that is constant across the emitter barrier and quantum well. Density distribution is not in steady state when the quasi-fermi level varies linearly across the quantum well. In the latter the steady state has negligible charge in the quantum well, see figure 9a. Figures 9b through 9f show temporal evolutions for the first 10fs. Notes: each figure incorporates the temporal evolutions of the proceeding figures. Thus (f) includes overlays of (a) through (e). The final state if figure 9a.

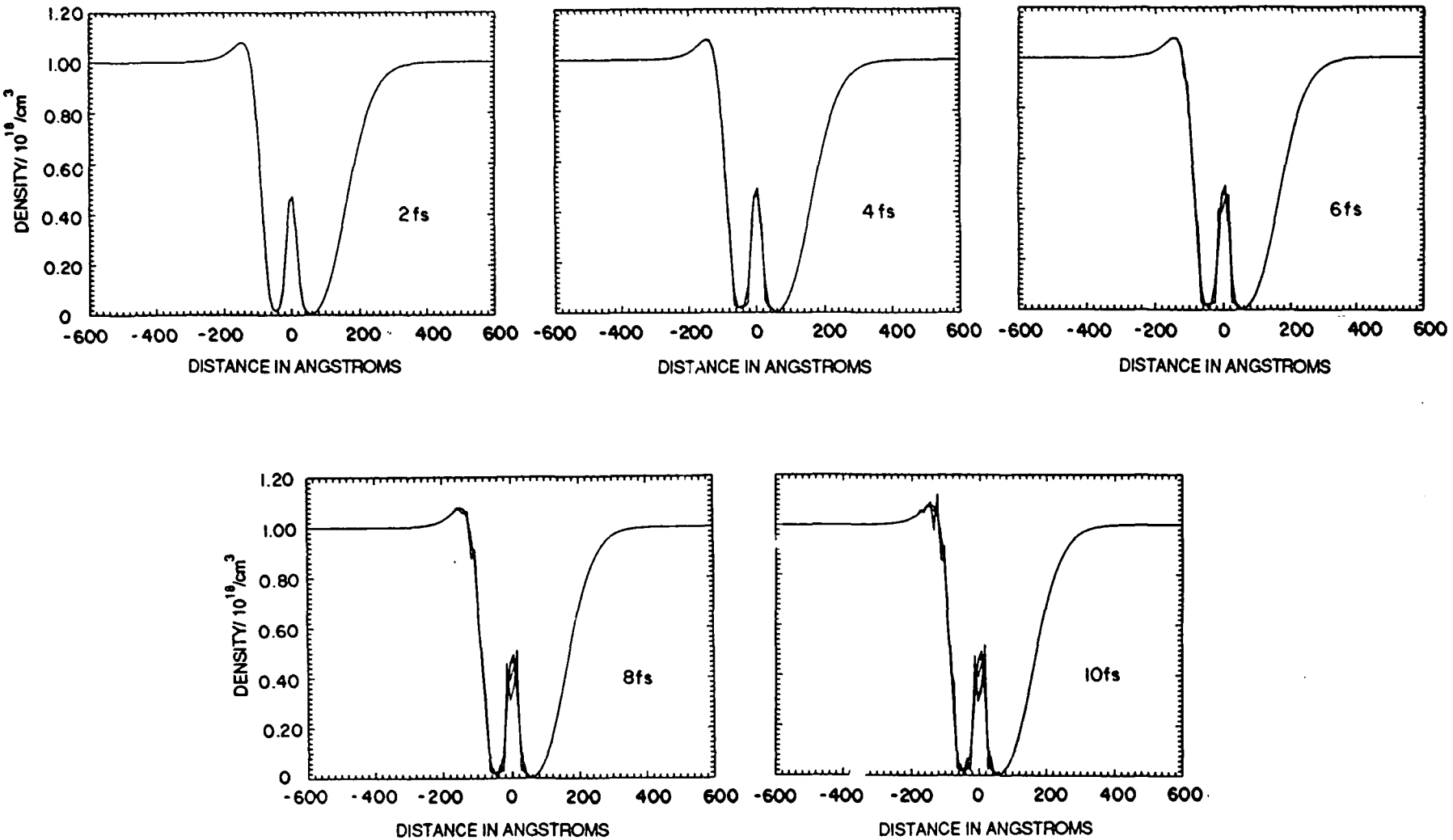

Figure 11. Space charge variations for constant quasi-fermi level across quantum well, and a bias of -200mev + 10mev sinωt, $\omega = 10^{14}$ radians/sec.

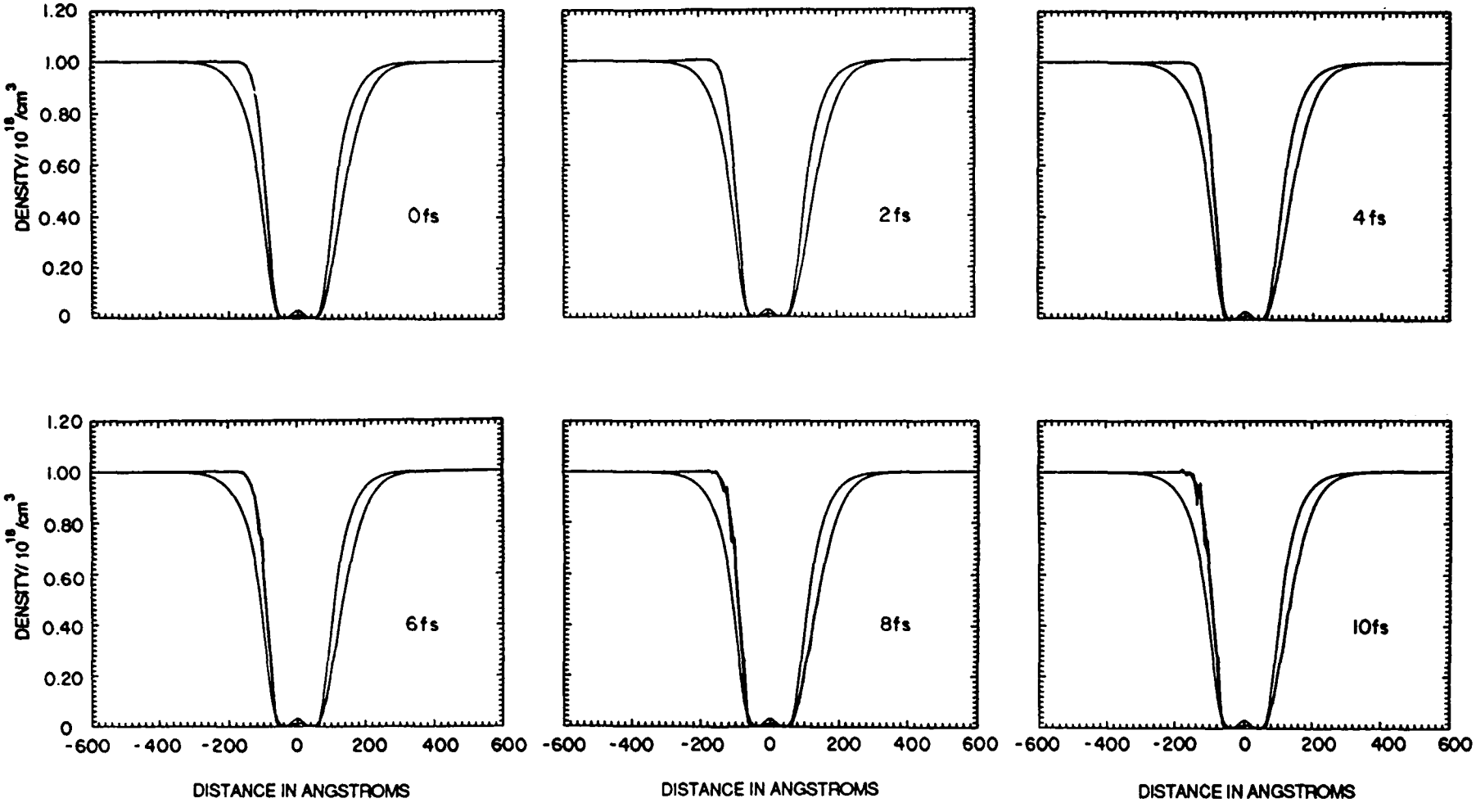

Figure 12. Space charge variations for linear quasi-fermi level across quantum well, and a bias of -200 mev + 10 mev sinωt, $\omega = 10^{14}$ radians/sec.

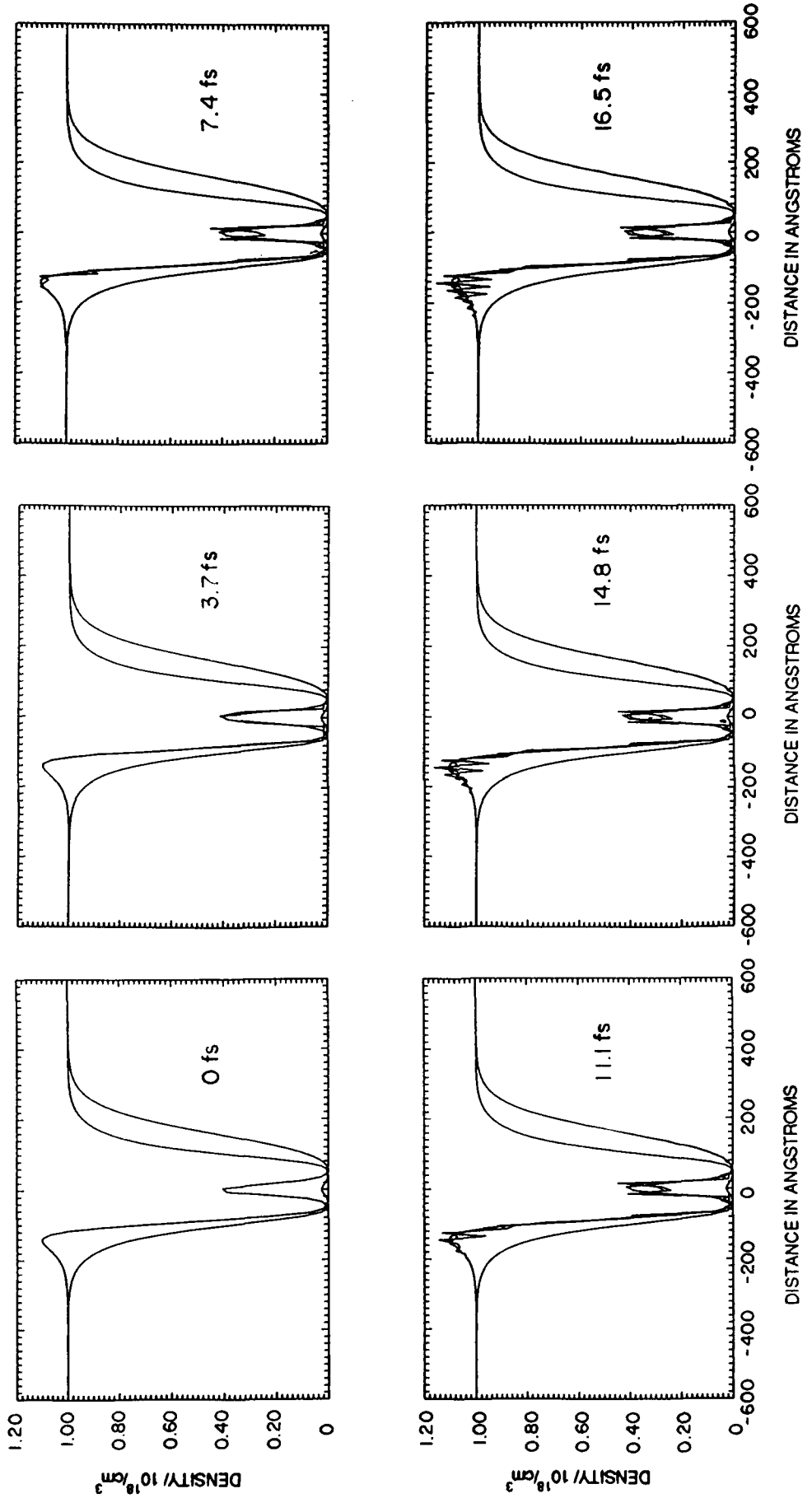

Figure 13. Space charge variations for constant quasi-fermi level across quantum well, and a bias of -200 mev + 10mev sinωt. $\omega = 2\pi f$. f = 54Thz.

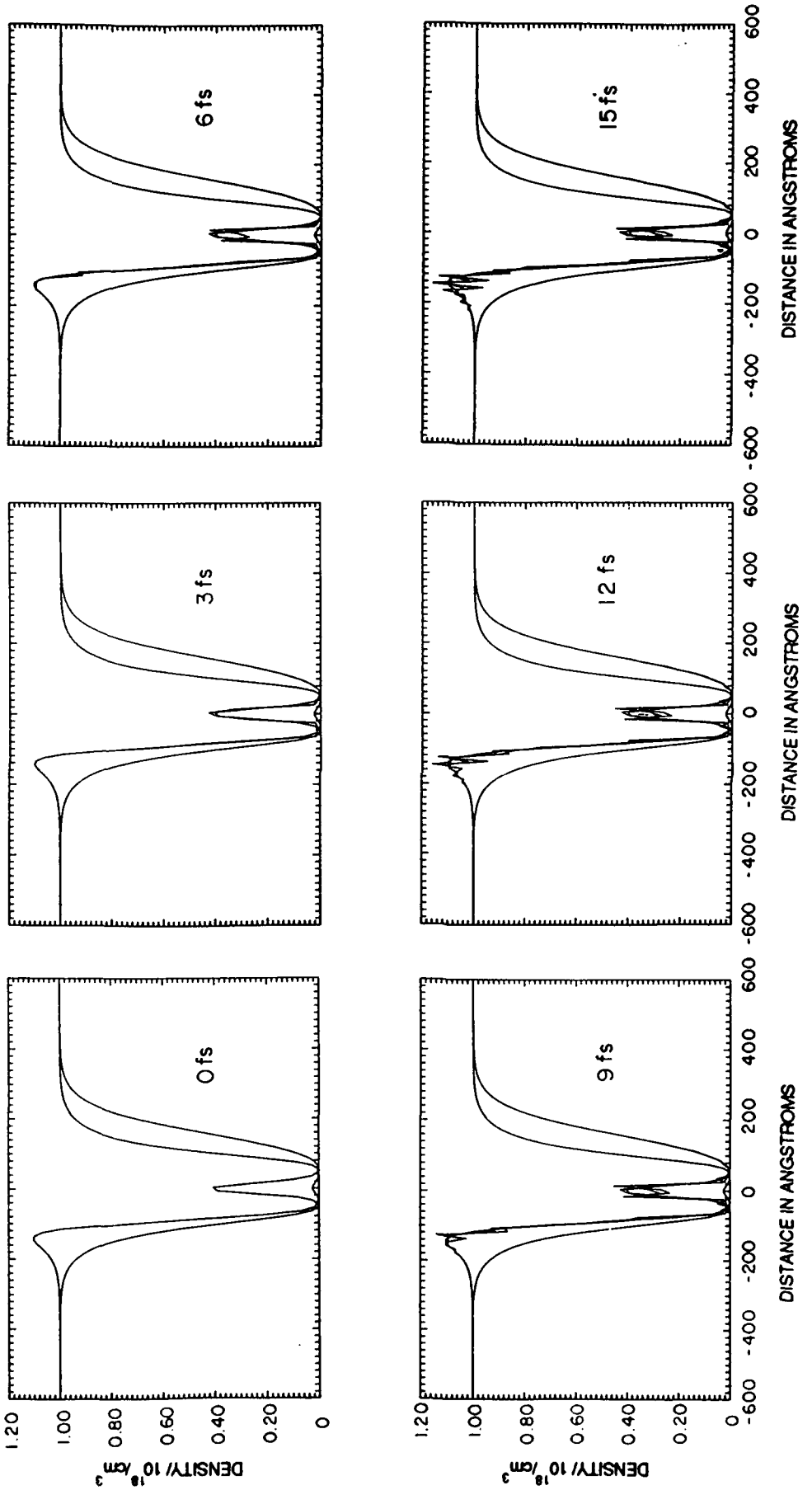

Figure 14. Space charge variations for constant quasi-fermi level across quantum well, and a bias of -200 mev + 10mev sinωt. f = 66THz.

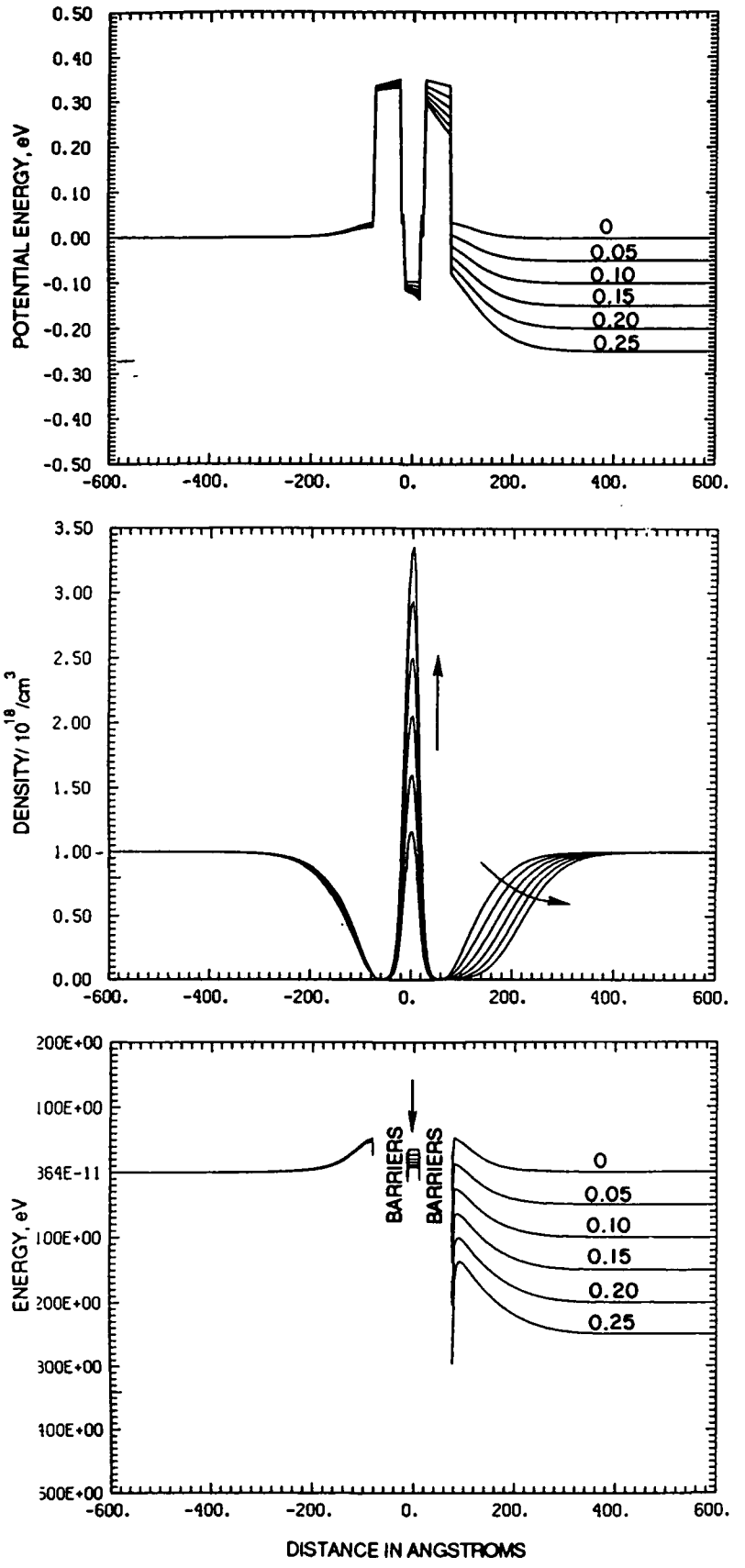

Figure 15. Steady state calculation for voltages to an estimated V_p, the voltage at peak current. (a) Potential energy vs. bias. Arrow points in direction of increasing collector bias. (b) Density vs. bias. Arrows point in direction of charge variation with increasing bias. (c) Quantum potential plus potential energy. Arrows point in direction of variation with increased bias.

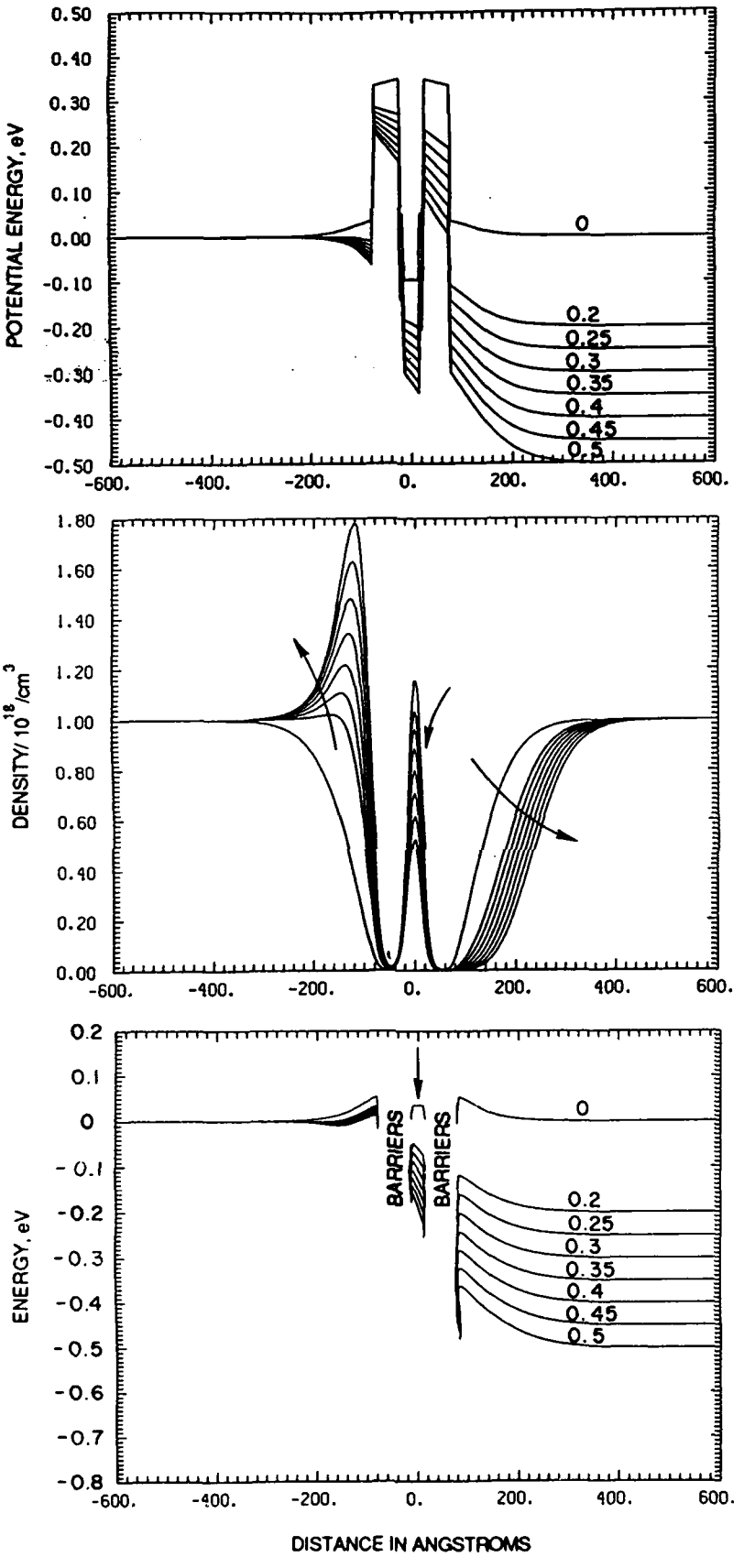

Figure 16. Steady state calculations for voltages beyond V_p, the voltage at peak current. (a) Potential energy vs. bias. Arrow points in direction of increasing collector bias. (b) Density vs. bias. Arrows point in direction of charge variation with increasing bias. (c) Quantum potential plus potential energy. Arrows point in direction of variation with increased bias.

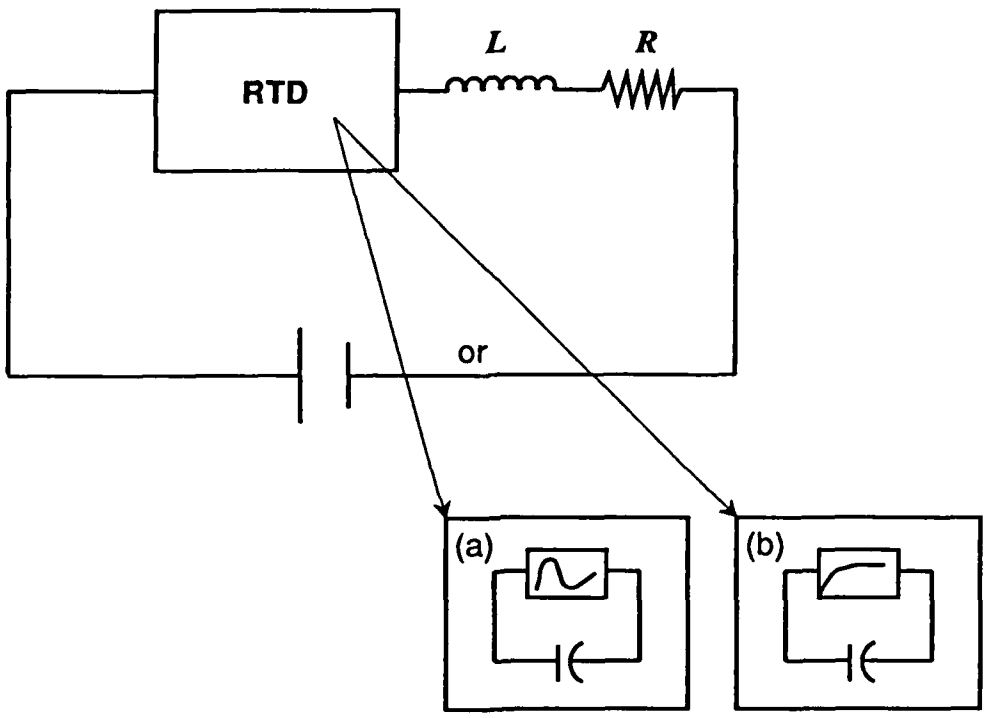

Figure 17. Schematic of a circuit in which an RTD would permit sustained circuit oscillations. Insets display equivalent circuit elements for (a) negative differential resistor in parallel with a voltage dependent capacitor, and (b) saturated resistor in parallel with a voltage dependent capacitor.

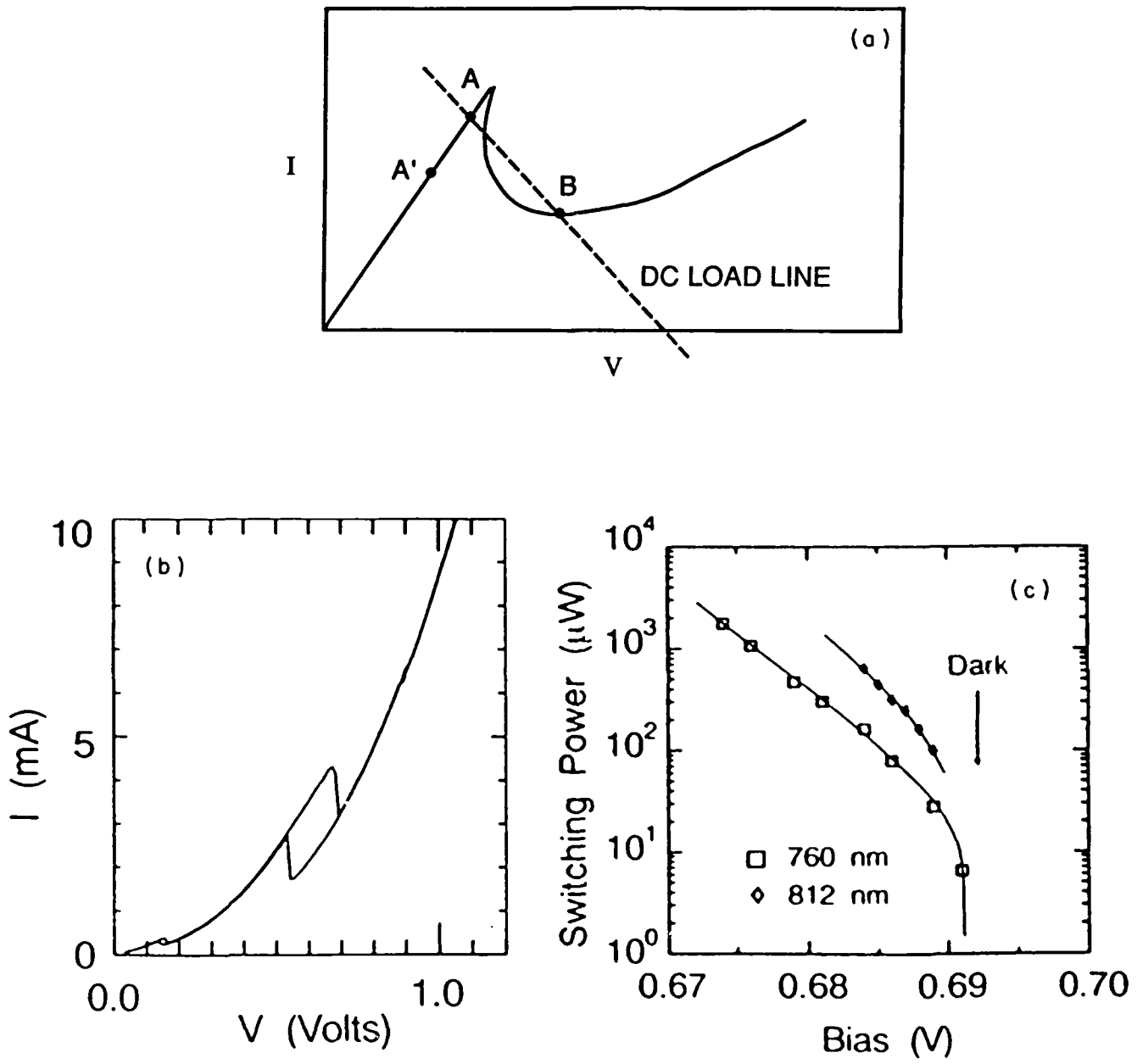

Figure 18. (a) The RTD as an optical switch. Device biased at steady point A. Illumination causes an increase in charge in quantum well, rearrangement of voltage within structure and switch along load line. To switch from A' requires more illumination. (b) Experimental IV curves of device that switched optically (England et al., 1991). (c) Switching power as a function of bias (England et al., 1991).

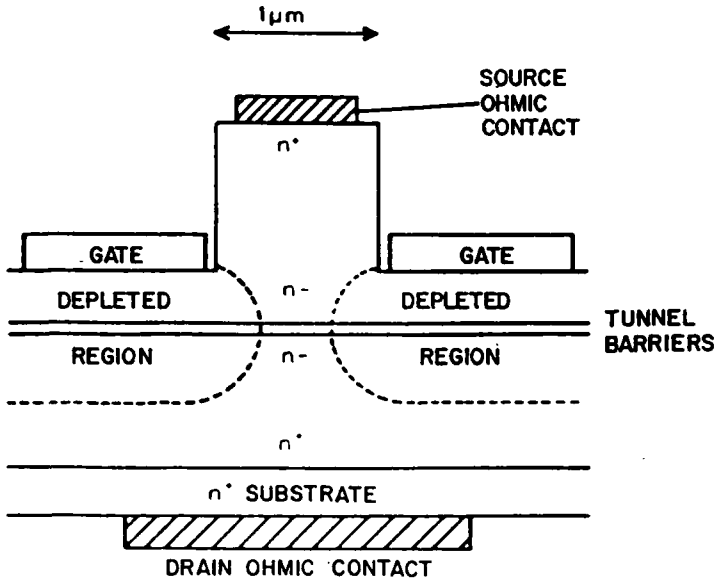

(a)

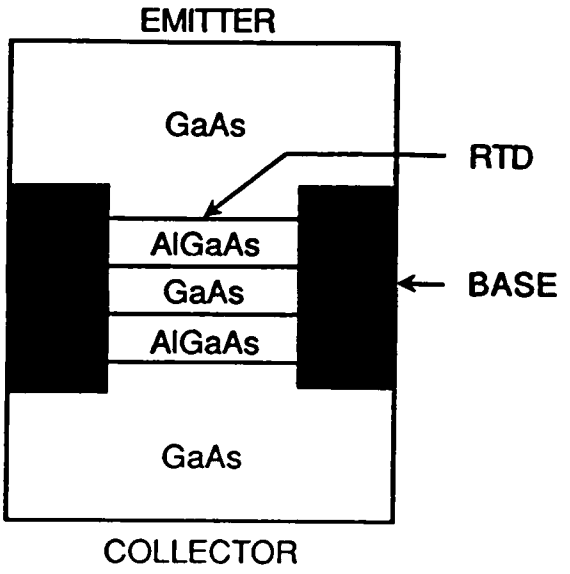

(c)

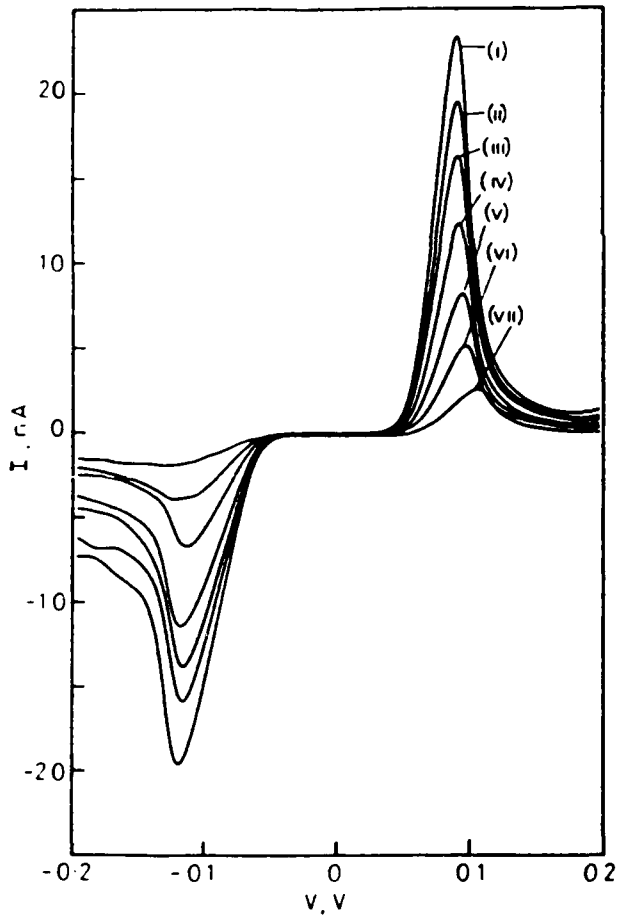

(b)

500nm GaAs n = 2 x 10^{18} cm^{-3}
200nm GaAs n = 2 x 10^{17} cm^{-3}
200nm GaAs n = 1 x 10^{17} cm^{-3}
300nm GaAs n = 4 x 10^{16} cm^{-3}
300nm GaAs n = 2 x 10^{16} cm^{-3}
3.4nm GaAs u.d.
5.7nm $Al_{0.4}Ga_{0.6}As$ u.d.
11.9nm GaAs u.d.
5.7nm $Al_{0.4}Ga_{0.6}As$ u.d.
3.4nm GaAs u.d.
300nm GaAs n = 2 x 10^{16} cm^{-3}
300nm GaAs n = 4 x 10^{16} cm^{-3}
200 nm GaAs n = 1 x 10^{17} cm^{-3}
200nm GaAs n = 2 x 10^{17} cm^{-3}
500nm GaAs n = 2 x 10^{18} cm^{-3}
n^+ SUBSTRATE

Figure 19. (a) Schematic of a vertical RTD FET (Dellow et al., 1991). (b) IV and structure of the RTD FET (Dellow et al., 1991). (c) One cell of a proposed RTD/PBT.